NATIONAL TRANSPORTATION SAFETY BOARD
Office of Research and Engineering
Materials Laboratory Division
Washington, D.C. 20594

March 7, 2008

MODELING GROUP REPORT

A. ACCIDENT

Place	:	Minneapolis, Minnesota
Date	:	August 1, 2007
Vehicle	:	I35W Highway Bridge
NTSB No.	:	HWY07MH024
Investigator	:	Gary Van Etten

B. DETAILS

This document contains the Modeling Group Contractor Interim Report dated February 14, 2008.

STRUCTURAL AND LOCAL FAILURE STUDY OF GUSSET PLATE IN MINNEAPOLIS BRIDGE COLLAPSE

Interim Report - NTSBC070010

Toshio Nakamura, Professor
Department of Mechanical Engineering
State University of New York at Stony Brook
Stony Brook, NY 11794-2300

Submitted to
National Transportation Safety Board
Washington D.C. 20594

February 14, 2008

Overview

The present study began in late September 2007 at SUNY Stony Brook. This effort is a collaborative investigation of NTSB, Stony Brook and Dassault Systems Simulia Corp. (SIMULIA). On October 10, a team of investigators from NTSB, Stony Brook and SIMULIA made a site-visit to inspect the re-assembled bridge structures in Minneapolis and a kick-off meeting was also held. Afterward, tele-conferences were held regularly (approximately every 2~3 weeks) to discuss work progress and identify key areas to investigate. Many of the tele-conferences were joined by the investigators from FHWA and MNDOT. Nakamura also met with the NTSB investigators (Dr. Schultheisz and Dr. Kushner) at the NTSB Training Center on January 23, 2008 to update the work and discuss areas to further study. Re-inspection of parts near U10W joint was also made at that time.

Modeling and analysis work began immediately after the site-visit in October. During the initial phase, the work was concentrated on elucidating the loads and deflections of main truss members connecting to U10W gusset plates using the global model supplied by FHWA. Subsequently, a "local" model representing the U10W joint was constructed with shell and solid 3D elements. This model was integrated into the global model to analyze the detailed stress and deformation behavior of the gusset plates. Since then, several modifications were made to improve the accuracy of local model representing the U10W region. The areas that were investigated closely were; geometric nonlinearity effect, elastic-plastic material behavior, coupling between beam and shell elements, attachments between gusset plates and trusses, contact condition, and resolutions of mesh. These efforts were also conducted in parallel with the progress and the modifications of global model by FHWA.

In the followings, issues regarding the present investigation efforts are summarized. Additional details can be found in the attached report from SIMULIA. Results that were not included in the SIMULIA report are also shown below.

Modeling/Mesh Issues

In the present study, finite element models are generated by FHWA and SIMULIA. Some computations were also carried out at Stony Brook. There were several issues related to finite element modeling of entire bridge and local U10W joint region.

Global Model

The FE model of entire bridge was made by FHWA, and subsequently modified following suggestions from SIMULIA as well as NTSB and Stony Brook. Initial concerns included the boundary conditions, element type selections, steel mass specifications and suitability of element sizes (i.e., number of beam element within one truss member). In addition, proper modeling of stringers on the deck, bridge barriers, and bridge pillars are closely examined. Most of these concerns were resolved in the subsequent models.

Element Types

Outside the local model, B31, B33, S4R, SPRINGA type elements are used to represent trusses, and other parts of the bridge. The local mesh is constructed with C3D20R elements for gusset plates and S4R for other members. C3D8 type elements were substituted for C3D20R in the analysis with contact conditions.

Coupling between Global and Local Models

The connections between beam elements to shell elements at the boundaries of global/local model may significantly influence the states of stress in the gusset plates. Two types of coupling conditions were considered, distributed load and kinematic. The former coupling resulted in large local deformations of trusses of the local model at their connecting locations. While the kinematic coupling may impose additional constraints (slightly increased stiffness of local model), this coupling was chosen at all the connecting locations to avoid the locally large deformations with the distributed load coupling.

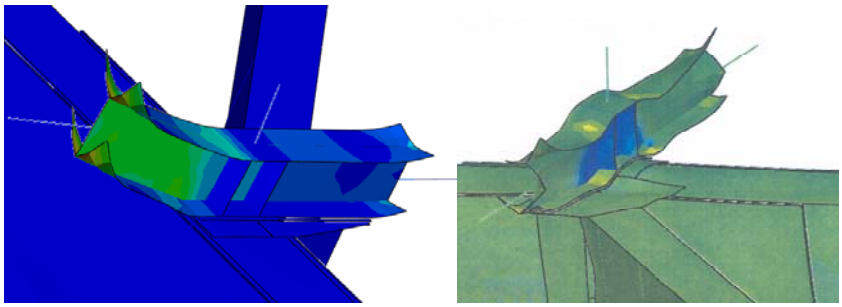

Fig. 1. Large local deformation of shell elements at ends with distributed coupling condition.

Stiffness of Joint Region

In order to assess the accuracy of stiffness of mode with only beam elements (all joints except U10W joint in the global/local model), the load-point-deformation behaviors were analyzed with unit load applications. The results were compared with those of the detailed 3D/shell model of

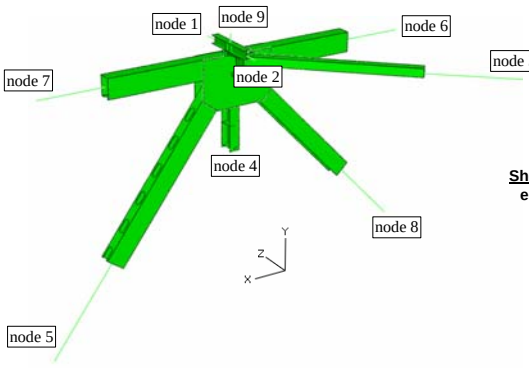

Fig. 2. Node labels for connections to U10W joint

Beam

end nodes	x	y	z	r1	r2	r3
1	9.01E-03	1.63E-03	2.22E-04	1.26E-06	6.05E-06	3.71E-03
2	7.08E-03	1.37E-03	2.16E-04	1.02E-06	3.63E-06	2.64E-03
3	1.52E-03	0.3154				
4	1.92E-02	2.19E-04	3.96E-03	6.53E-07	6.86E-03	3.78E-06
5	4.72E-04	2.60E-04	3.57E-02	6.01E-07	1.02E-06	4.18E-07
6	2.02E-04	1.27E-02	1.26E-02	5.60E-06	4.17E-07	4.43E-07
7	1.75E-04	1.06E-02	1.05E-02			3.52E-07
8	4.19E-04	3.81E-04				
9	3.11E-03	1.01E-04				

Shell/Solids with All Kinematic Couplings

end nodes	x	y	z	r1	r2	r3
1	5.66E-03	**2.12E-03**	1.94E-04	**1.61E-06**	5.33E-06	1.30E-03
2	2.46E-03	1.30E-03	1.82E-04	**1.29E-06**	3.05E-06	9.12E-04
3	1.56E-03	0.2395				
4	4.68E-03	1.67E-04	**5.11E-03**	**9.31E-07**	4.10E-05	2.53E-06
5	**4.78E-04**	**2.64E-04**	**3.77E-02**	**6.61E-07**	**1.13E-06**	3.88E-07
6	1.81E-04	8.69E-03	1.20E-02	4.27E-06	**4.39E-07**	3.99E-07
7	1.61E-04	7.76E-03	**1.08E-02**			3.23E-07
8	3.99E-04	3.64E-04				
9	2.11E-03	**1.12E-04**				

black: close green: ~5%off bue: ~10%off red: 20%off brown: 30%+off

bold/underline shell model more compliant

Table 1. Stiffness comparison of beam only model and detailed model

the U10W joint as shown in Fig. 2. The Table 1 shows the displacements and rotations of nine connecting points for "beam-only" model and "solid/shell/beam" model. At some degrees of freedom, the differences between the two models are significant. However, as the Table 2 (from the beam only global model) on the right indicates, the large loads/moments are transmitted through trusses to U9, L9, U11, L11 joints (nodes 7, 5, 6, 8, respectively). At these connecting locations, the differences are somewhat lower though still not negligible.

Mesh Refinement

In the initial global model, a limited number of beam elements were used for each truss member regardless of its actual length. To increase the accuracy of deformation near the U10W joint, additional elements were added in the trusses connecting the joint. Within the local model, mesh representing gusset plates were also refined (see attached report from SIMULIA for details). With the refined model with 0.1" as the smallest in-plane element size, the maximum stress level

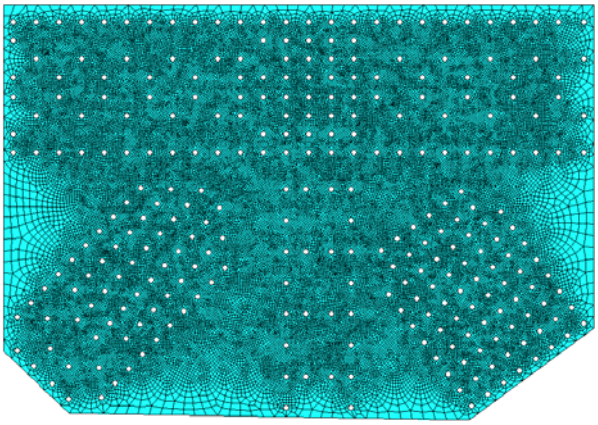

Fig. 3. A sample gusset plate mesh with rivet holes.

	Forces (klb)		Moments (klb.in)	
Truss	Axial	Shear	Twist	Bend
node 7	1831	5.1	-37	185
node 5	-2355	11.8	64	2666
node 4	396	3.3	0	84
node 8	1904	6.7	-1	1513
node 6	-741	16.2	-7	3472

Table 2. Load and moments of main trusses to U10W joint

increased appreciably. However, the stress distributions within the gusset plates remained similar to those of 0.5" element model. In order to model every rivet hole in a gusset plate, a large number of elements would be required. A sample mesh shown in Fig. 3 contains about 50,000 in-plane elements. If 3D elements were used to model, a minimum of 200,000 C3D8 elements would be required for a single gusset plate. Thus, the next step in the mesh refinement is planned using a sub-model (selected region of U10W joint) to resolve accurate stress states.

Material and Geometrically Nonlinear Issues

Initially, linear elastic material properties were assumed for all the parts in the bridge. Then the elastic-plastic tensile measurements of actual gusset plate were supplied by NTSB, and they were included in the subsequent elastic-plastic analysis. Several analyses were also performed with and without imposing the "nonlinear geometry" condition.

Elastic-Plastic Properties of Gusset Plates.

Based on the uniaxial tensile test data provided by NTSB, the steel properties are chosen as,

Elastic Modulus	Poisson's Ratio	Density	Yield Strength	Ultimate Tensile Strength
29,000ksi (200GPa)	0.3	8.37625×10^{-7} kip.sec^2/in^4 (8945 kg/m^3)	51.5ksi (355MPa)	80.0ksi (552MPa)

Also the NTSB tests estimated the uniaxial failure strain to be well over 15%. In the present finite element analysis, the stress-strain relation is idealized as a piece-wise linear model with σ = 51.5ksi at yielding, σ = 75ksi at ε^p = 0.04, σ = 88ksi at ε^p = 0.10, and non-hardening for ε^p > 0.10. These values correspond to Cauchy stresses and true plastic strains, respectively.

Nonlinear Geometry

Although magnitudes of strains are expected to remain small, effects of large rotations may influence the deformation states of the entire bridge structures. The comparison of results from the linear geometry model (small strain/displacement assumption) and the nonlinear geometry model predicted up to 10% difference in the truss loads connecting into U10W joint. Since these variations were not trivial, the nonlinear geometry effects are included in the most of the analyses.

Possible Failure Mechanisms

Although the investigations have focused on the stress and deformation states surrounding the U10W joint, the present study has also monitored other locations of the bridge for large stresses and potential instability conditions. In order to identify possible failure models, the loads were artificially increased beyond the currently estimated final loads. The initial study predicted an increase 5-10% of final load magnitude initiated computational divergence. The causes of such a divergence will be investigated closely in the next phase of the contract.

Structural Instability

Using the global model provided by FHWA, a buckling analysis was carried out to examine the possible instability of trusses and other member under large compressive loads. The computed critical buckling loads were significantly higher than the estimated final load applied on the bridge. However, this analysis was carried out with a perfect geometry model, and small misalignments or perturbed trusses may reduce the critical loads for buckling.

Material Instability

Large plastic deformation or shear localization may initiate failure of gusset plates. With the present models, estimated strains are well below the measured failure strain under uniaxial condition. Although gussets themselves are compliant, attachments of stiff trusses at large areas of plates add rigidity to the gussets and deformation is constrained. A further study using a refined sub-model of gusset plate will provide better estimates of localized deformation states, especially near rivet holes.

Crack Initiation and Growth

Based on the measured ductility of the steel and visual inspections of the fractured surfaces of the gusset plates, all crack propagations appears to be *ductile*. Thus, a *sizable* crack growth prior to the structural failure may not be likely. However, a limited crack initiation and growth near rivet holes may be possible. Based on computed stresses in the sub-model, a crack propagation model with cohesive elements may be incorporated in the model to study the possibility. Such a simulation will require fracture toughness of the gusset plate material.

Future Investigations

Based on the analyses performed up to now, future investigations will be concentrated on the following areas.

- Construction of sub-model for a section of the gusset plate (through the thickness as well as in-plane) including selected rivets and holes.
- Identification of sources of divergences observed under artificially increased load.
- Further refinement of contact conditions between the gusset plate and the edges of the truss members.
- Effects of friction between the gusset plate and the edges of the truss members.
- Effect of initial imperfection shown by bowing in the gusset plates. The 3D model will be modified to assess this effect.
- Eccentricity in the floor truss connection between U10W and L10W joints where 5 members are connected.
- Construction of L11W joint model to study the effect of corrosion.
- Thermal expansion effects.

PIN07-041

A Technical Report for:

I-35 Bridge Gusset Analyses

January 25, 2008

Submitted to:

Prof. Toshio Nakamura

Department of Mechanical Engineering
State University of New York
Stony Brook, NY 11794-2300

Prepared by:

Dassault Systemes Simulia Corp.
SIMULIA Central
1440 Innovation Place
West Lafayette, IN 47906

SIMULIA

Executive Summary

SIMULIA Central performed nonlinear finite element analyses on the Minneapolis I-35W bridge using an embedded three dimensional (3D) local model of the U10W joint. The model was analyzed using the original design bridge weight, additional concrete weight, and construction loads determined at the time of collapse. The analyses focused on predicting the stress distribution in the gussets of the U10W joint. The global bridge models were provided by the Federal Highway Administration (FHWA).

The 3D local model consisted of two gussets, five main trusses, one lateral brace, one floor truss, and other connecting components. The gussets were represented with solid hexahedron elements while all other components in the local model were represented with shell elements. Isotropic elasto-plasticity was assumed for all components.

Rivets connecting the gussets to the five main trusses were represented with the "fastener" feature available in the Abaqus finite element software. All other connections between components were represented with tie constraints.

Two contact scenarios were examined: with and without contact defined between the gussets and the diagonal truss perimeters. No other boundary conditions were defined in the local 3D model. The five main trusses, lateral brace, floor truss and stringer offset were cut at about mid-span of the global model members. Tie and coupling constraints were introduced at the cut planes to connect the local 3D U10W model to the global bridge model.

The effect of the embedded local 3D U10W model on the response of the global bridge model was examined by performing linear analyses on two global models: the original model (given by FHWA) and the mixed model (with the embedded 3D local model). The analyses predicted small differences in mass, reaction forces, displacements at U10W and U10E nodes, and truss internal forces at U10E node. This implied that the effect of the embedded local 3D U10W model on the global model is insignificant.

The nonlinear analyses predicted no apparent plastic deformation in any of the trusses in the bridge when subjected to construction loads. Plastic deformation mainly occurred in the two gussets at the U10W node. Plastic deformation was predicted to occur in the gusset region outside of the top row of fasteners connecting the U10_L9W truss. The plastic deformation was apparent beginning in the initial load condition of the originally designed bridge, although only a few elements yielded through the entire gusset thickness. With the application of additional concrete weight and construction loads, more elements yielded through the entire gusset thickness.

Using a mesh density seed of 0.1 inch, the maximum predicted stress due to construction loads was 77 ksi and occurred on the west face of the east gusset. This corresponded to a predicted equivalent plastic strain of 4.3%. The predicted deformed shape of the gussets indicated that the west face of the diagonal truss U10_L9W was prone to move transversely outward of the bridge while the east face of the truss U10_L9W moved inwards towards the bridge.

Mesh density and its effect on the gusset stress predictions were also investigated. A refined mesh predicted somewhat higher stresses, as expected. Mesh convergence could be investigated further using the submodeling method of Abaqus.

Finally, a preliminary study on the effect of contact interactions between the gussets and truss perimeter was conducted. Initial results indicated that contact conditions predicted slight lower stresses than the condition where the gusset and trusses were fastened at their interfaces and no contact was defined. Note that the effects of gusset holes and three-dimensional rivets have not been analyzed. More complex analyses involving actual rivets and holes could be investigated further.

Introduction

The National Transportation Safety Board (NTSB) has been investigating the collapse of the Minneapolis I-35W bridge. The Federal Highway Administration (FHWA) has been performing analyses of the bridge using whole bridge models built of structural elements such as beam and shell elements. The beam elements were used to represent trusses and the shell elements were used to represent concrete decks and piers. These models provide insight into the loads and load paths in the bridge, but do not provide detailed results in specific regions such as gusset joints. To assist the investigation, SIMULIA Central was subcontracted by SUNY Stony Brook, working under the direction of Professor Toshio Nakamura.

SIMULIA Central focused on the gusset joint at the U10W bridge node and created a detailed local model of the joint. This detailed local model of the gusset joint was embedded into the bridge model provided by FHWA so that stress and strain in the gussets could be evaluated in more detail. This report describes the nonlinear large deformation analyses of the gusset joint using Abaqus software.

Summary of Bridge Global Models Provided by FHWA

Four global models of the whole I-35W bridge were provided by FHWA. The first model was provided in October 2007, the second one in November 2007, the third one in December 2007, and the fourth one in January 2008. FHWA included slight modifications in each model iteration as more information was available and better techniques were incorporated. SIMULIA Central reviewed the first two models and used the second model to drive a three-dimensional (3D) local model representing the gusset joint at the U10W node. The most recent FHWA bridge model has not yet been used to analyze the U10W gusset in detail.

The first FHWA model had eight analysis steps. It ran smoothly and quickly if linear geometry was assumed. However, when nonlinear geometry was incorporated, the analysis diverged in the beginning of the analysis. The issue was resolved by specifying specific normal directions to those beams that form a curved path.

The second FHWA model [1] consisted of B31, B33, S4R, and SPRINGA elements, as shown in Figure 1. The B31 elements represented stringers. The B33 elements represented trusses and short vertical beams used as stringer offsets. The S4R elements represented concrete decks and piers. The SPRINGA elements represented the effect of approach spans on the main trusses.

Three loading steps were included in the second model. In the first step, piers were removed from the model, approach span loads were applied, and gravity loading was applied to the main trusses, concrete decks, and barriers. In the second step, piers were added and additional loads were applied to reflect added concrete and modified barriers through the life of the bridge. In the third step, construction loads at collapse were added.

Local 3D Model Description

Nonlinear Static Analysis

Abaqus/Standard version 6.7 was used to perform nonlinear static finite element analyses to predict the distribution of stress and strain in the gussets at the U10W node. Analyses were performed using the same load conditions applied in the global bridge model supplied by FHWA. These load conditions included the weight of the bridge as originally designed, the weight of the bridge with additional concrete from prior design modifications, and the weight of the modified bridge with additional construction loads at the time of collapse.

Geometry and Meshing

NTSB provided original and reproduced drawings of gussets, truss members, lateral brace, fasteners and their positions, and additional details as summarized in Table 1. Also provided were two CAD models, in Abaqus CAE format, of the gusset joints at the U10W and U10E nodes, as summarized in Table 1. Figure 2 shows the CAD model of the gusset joint at the U10W node. The CAD model consisted of two identical gusset plates, two horizontal main trusses, two diagonal main trusses, one vertical main truss, one lateral brace, one floor truss and other connecting components such as spacers, splice plates, lateral plates, I-stiffener, diaphragms, etc. These components are summarized in Table 2.

Table 1
CAD Data of the Gusset Joints at U10W and U10E nodes

File Type	File Name	Date
Drawing	Minnosota.pdf	10-09-07
Drawing	BR9340 Construction Plan (1965).pdf	10-25-07
Drawing	BR9340 Steel Details (1965).pdf	10-25-07
CAD Model	U10_west.cae	10-25-07
CAD Model	U10_east.cae	10-26-07

Table 2
Components in U10_west.cae

Type	Component 1	Component 2	Component 3
Gusset	U10W_Gusset_W	U10W_Gusset_E	
Horizontal Truss	U10_U9W	U10_U11W	
Diagonal Truss	U10_L9W	U10_L11W	
Vertical Truss	U10_L10W		
Lateral Brace	U10W_CU11		
Floor Truss	U10W_FT		
Internal Filler Plate	U10W_fill_W	U10W_fill_E	
Internal Splice Plate	U10W_splice_W	U10W_splice_E	
External Splice Plate	U10W_splice_top	U10W_splice_bottom	
Plate Supporting Lateral Brace	U10W_lateral_top	U10W_lateral_bottom	U10W_lateral_angle
Floor Truss Support	U10W_FT_support		
Diaphragm A	U10W_diaphragmA		
I_Stiffener	U10W_I_stiffener		

The 3D local model of the gusset joint at the U10W node included all the components displayed in Table 2, as shown in Figures 3 and 4. The gussets were represented with C3D20R elements, which are 20-node quadratic brick and reduced integration elements. All other parts in the 3D local model were represented by S4R elements, which are 4-node doubly curved general-purpose shell and reduced integration elements. The five main trusses, lateral brace, floor truss and stringer offset were cut at about mid-span of the global model members, exactly at the nodal positions of the center beam element in the span, as shown in Figure 3. The element number of the five main trusses in the global model was increased. Figure 4 displays all other components except the gussets, five main trusses, lateral brace and floor truss.

Material Properties

One type of steel material was used for all components in the local model. The steel was represented as an isotropic elasto-plastic material with the material properties shown in Table 3 and Figure 5.

The steel stiffness, strengths, and ultimate tensile strain were provided by NTSB. NTSB obtained these values from tensile tests of steel specimens cut from the actual bridge gussets. The density shown in Table 3 and used in the global bridge model was provided by FHWA within the global bridge model. Note that this density is artificially high to account for mass not

modeled in the bridge model. The density of steel used in the local U10W model was the same as the density used in the global bridge model. In the future, the steel density used in the 3D local model should be 7.298 x 10^{-7} kip*sec^2/in^4.

Table 3
Material Properties of Steel Used in the Bridge Model

Material	Elastic Modulus (ksi)	Poisson's Ratio	Density (kip*sec^2/in^4)	Yield Strength (ksi)	Ultimate Tensile Strength (ksi)	Ultimate Tensile Strain
Steel	2.9 x 10^4	0.3	8.37625 x 10^{-7} *	51.5	80.0	0.1

The density will be 7.298 x 10^{-7} kipsec^2/in^4 in the future analyses.

Constraints, Rivets, Contacts and Boundary Conditions

The cut planes of the five main trusses, lateral brace, floor truss and stringer offset were located at a position corresponding to a nodal position in the global model, as described above. Nine reference points coincident with these nodes were added and tie constraints were applied to them, as shown in Figures 3 and 6. These reference points were then coupled to the cut planes of the shell truss representations, as shown in Figure 7. The two couplings for the floor truss and the coupling for the lateral brace were distributing couplings while all other couplings were kinematic couplings. The introduction of the distributing couplings was implemented since the global nodes and centers of the three cut planes were not coincident. As modeled, the entire 3D local model was embedded into, and driven by, the global model.

All rivets connecting the gussets and the five main trusses were represented by Abaqus fasteners, as shown in Figure 8. Abaqus fasteners provide a simplified method to connect several components without having to model the actual fastener in detail. In Abaqus fasteners, nodes within a specified radius of influence on one component are automatically coupled to nodes within the specified radius of influence on another component, thereby fastening the components together. In the local 3D model, the fasteners were defined to have a radius of influence of 0.5 inch, which coupled an adequate number of nodes in the fastener region.

All other connections between components in Table 2 were represented by tie constraints. Initially, no contact was added. Later, contact pairs were defined between the gusset plates and the perimeter of the adjacent diagonal trusses. This allowed an initial investigation into the effect of contact on the stress distribution in the gussets. Figure 9 shows the contact regions defined in the local model. A Coulomb friction model was used with a friction coefficient of 0.1.

No translational or rotational boundary conditions were defined in the local 3D model.

Loading Conditions

The local 3D model representing the U10W joint was embedded into the second (November 2007) global bridge model [1] and was driven by global model loads transferred through the tie and coupling constraints defined above. As described previously, there were three loading steps: original bridge weight, additional concrete weight, and construction load at collapse. These

loads were applied using a combination of gravity load, line loads, concentrated loads, and pressure

Effect of Embedded 3D Local Model on Bridge Global Model

Small-Displacement Analysis

To investigate the effect of the embedded 3D local model on the global bridge model, small-displacement analyses were performed on the second global bridge model. The global model was analyzed in two ways. First, it was analyzed as given by FHWA. Second, it was analyzed with the 3D local model included. Results of the two models were then compared to determine the effect of the embedded local model.

For the sake of convenience, the global bridge model provided by the FHWA was called the original model and the global bridge model with the embedded 3D local model was called the mixed model. In the original and mixed models, the steel property was initially assumed elastic.

Comparison of Mass

Table 4 shows the comparison of total mass and the center of mass between the original and mixed models. As shown, the difference was very small and is most likely due to the differences in density described above.

Table 4
Comparison of Mass between Original and Mixed Models

		Mass (kip*sec^2/in)	Center of Mass (in)
Step 1	Original Model	41.277	6344.166, -25.41205, 1301.853
	Mixed Model	41.283	6344.430, -25.41353, 1301.914
Step 2 & 3	Original Model	66.758	6177.428, -390.3247, 1301.909
	Mixed Model	66.764	6177.606, -390.2932, 1301.947

Comparison of Reaction Forces in Step 3

The boundary conditions in step 3 are shown in Figure 10, where the red numbers show the node labels for nodes that have assigned boundary conditions. Table 5 presents the original and mixed model reaction forces predicted from step 3 (construction loads) of the analyses. Forces and moments in black are from the original model while the forces and moments in blue are from the mixed model. Table 6 provides the difference in the forces and moments between the two models. Almost all forces and moments had less than 5% difference. Six out of sixty forces and moments had differences greater than 5%. All six differences were small in terms of absolute values of forces and moments.

Table 5
Original and Mixed Model Reaction Forces Comparison, Step 3 (Construction Loads)

Node Label	RF1 (kip)	RF2 (kip)	RF3 (kip)	RM1 (kip*in)	RM2 (kip*in)	RM3 (kip*in)
171	-16.06*	1293	11.58	3504	16.12	5944
	-16.07*	1297	11.37	3439	20.64	5942
178	-16.16	1260	10.16	3328	31.56	6073
	-16.29	1263	9.959	3263	36.08	6136
273	9.286	1631	0.281	44.66	-81.73	-8727
	9.297	1632	0.345	73.88	-81.29	-8737
274	10.01	1674	-0.66	-173.1	-76.61	-9293
	10.02	1675	-0.6	-143.9	-76.17	-9301
368	-255.1	4721	57.04	-9134	-4084	123920
	-255	4719	57.05	-9075	-4086	123880
629	-295.4	4902	-45.5	10386	3644	138290
	-295.4	4852	-45	10338	3643	138370
633	285.3	4480	-111	14270	-6303	-167510
	284.5	4473	-111	14244	-6315	-167230
727	269.9	4429	112.3	-14107	6562	-162300
	270.7	4427	112	-14106	6549	-162560
11343	0	4.54	0			
	0	4.522	0			
11344	0	2.709	0			
	0	2.698	0			
11345	0	2.166	0			
	0	2.087	0			
11349	0	1.91	0			
	0	1.847	0			

*from the original model; *from the mixed model.

Table 6
Original and Mixed Model Reaction Force Difference, Step 3 (Construction Loads)

Node Label	ΔRF1 (%)	ΔRF2 (%)	ΔRF3 (%)	ΔRM1 (%)	ΔRM2 (%)	ΔRM3 (%)
171	0.1	0.3	-1.8	-1.9	28.0	0.0
178	0.8	0.2	-2.0	-2.0	14.3	1.0
273	0.1	0.1	22.9	65.4	-0.5	0.1
274	0.1	0.1	-9.7	-16.9	-0.6	0.1
368	0.0	0.0	0.0	-0.6	0.0	0.0
629	0.0	-1.0	-1.3	-0.5	0.0	0.1
633	-0.3	-0.2	0.1	-0.2	0.2	-0.2
727	0.3	0.0	-0.3	0.0	-0.2	0.2
11343	0.0	-0.4	0.0			
11344	0.0	-0.4	0.0			
11345	0.0	-3.6	0.0			
11349	0.0	-3.3	0.0			

Comparison of Displacements at U10W and U10E Nodes

Comparison of displacements at the U10W node between the original and mixed models is shown in Figures 11 and 12. Comparison of displacements at the U10E node between the two models is shown in Figures 13 and 14. Figures 11 and 13 compare the translational displacements while Figures 12 and 14 compare the rotational displacements. The solid curves in the figures were from the original model while the dots were from the mixed models. Very small difference was observed in the displacements at the two nodes between the two models.

Comparison of Truss Internal Forces at U10E Node in Step 3

Table 7 shows truss internal forces and moments at the U10E node in the original and mixed models, respectively. The forces and moments in black are from the original model while the forces and moments in blue are from the mixed model. The difference between the internal forces and moments is shown in Table 8. It implies that the difference was small, except for the moments of U10_U9E and U10_U11E trusses with respect to the global Y axis.

Table 7
Comparison of Truss Internal Forces at U10E Node in Step 3 between Original and Mixed Models When Using Small-Displacement Analyses and Elasticity of Steel

Truss	NFORC1 (kip)	NFORC2 (kip)	NFORC3 (kip)	NFORC4 (kip*in)	NFORC5 (kip*in)	NFORC6 (kip*in)
U10_L10E	1.584	-370.1	-4.43	75.13	0.2688	-5.96
	1.504	-369.6	-4.448	76.01	0.2687	-10.27
U10_U11E	672	-16.25	-0.3827	8.966	-22.92	3318
	664	-16.24	-0.1526	10.43	30.16	3317
U10_U9E	1796	-5.934	-0.3078	20.39	144.8	-335.7
	1794	-5.974	-0.0557	24.62	61.94	-345.6
U10_L11E	-1253	-1322	1.743	-647.9	616.7	939.1
	-1249	-1317	1.802	-660.4	628.5	942.2
U10_L9E	-1344	1798	2.397	-1096	-741.1	-2157
	-1341	1792	2.467	-1113	-755.6	-2157

Table 8
Difference in Truss Internal Forces at U10E Node in Step 3 between Original and Mixed Models When Using Small-Displacement Analyses and Elasticity of Steel

Truss	ΔNFORC1 (%)	ΔNFORC2 (%)	ΔNFORC3 (%)	ΔNFORC4 (%)	ΔNFORC5 (%)	ΔNFORC6 (%)
U10_L10E	-5.1	-0.1	0.4	1.2	0.0	72.3
U10_U11E	-1.2	-0.1	-60.1	16.3	-231.6	0.0
U10_U9E	-0.1	0.7	-81.9	20.7	-57.2	2.9
U10_L11E	-0.3	-0.4	3.4	1.9	1.9	0.3
U10_L9E	-0.2	-0.3	2.9	1.6	2.0	0.0

The above comparisons imply that the effect of the embedded local 3D model at the U10W node on the global model is small. One major concern might be the load redistribution from the soft U10W node to the stiff U10E node because of plastic deformation in the local model that is not

present in the global model. Tables 9 and 10 compare the truss internal forces at the U10E node when large-displacement analyses were performed and plasticity of the steel was introduced. Tables 8 and 10 show that load redistribution from the soft U10W node to the stiffer U10E node is insignificant.

Table 9
Comparison of Truss Internal Forces at U10E Node in Step 3 between Original and Mixed Models When Using Large-Displacement Analyses and Plasticity of Steel

Truss	NFORC1 (kip)	NFORC2 (kip)	NFORC3 (kip)	NFORC4 (kip*in)	NFORC5 (kip*in)	NFORC6 (kip*in)
U10_L10E	2.0	-371.2	-4.6	46.0	0.6	-68.2
	1.9	-371.9	-4.6	48.6	0.6	-72.1
U10_U11E	686.2	-12.2	-0.6	5.8	-101.3	3291.0
	679.8	-12.3	-0.4	8.5	-43.5	3292.0
U10_U9E	1788.0	2.0	-0.1	17.8	54.0	-194.6
	1788.0	2.0	0.1	19.9	-23.4	-200.0
U10_L11E	-1249.0	-1329.0	1.4	-724.1	682.1	959.0
	-1246.0	-1326.0	1.6	-732.4	690.0	961.0
U10_L9E	-1351.0	1793.0	2.6	-950.7	-639.2	-2278.0
	-1350.0	1791.0	2.6	-975.9	-659.9	-2280.0

Table 10
Difference in Truss Internal Forces at U10E Node in Step 3 between Original and Mixed Models When Using Large-Displacement Analyses and Plasticity of Steel

Truss	ΔNFORC1 (%)	ΔNFORC2 (%)	ΔNFORC3 (%)	ΔNFORC4 (%)	ΔNFORC5 (%)	ΔNFORC6 (%)
U10_L10E	-4.1	0.2	1.0	5.8	2.1	5.6
U10_U11E	-0.9	0.4	-37.5	46.7	-57.0	0.0
U10_U9E	0.0	-3.3	-225.6	11.6	-143.3	2.8
U10_L11E	-0.2	-0.2	10.3	1.1	1.2	0.2
U10_L9E	-0.1	-0.1	0.1	2.7	3.2	0.1

Analysis Results

Analysis results predict that no apparent plastic deformation occurs in any bridge trusses, as shown in Figures 15 and 16. Only a few spots in the trusses of the local 3D U10W model had von Mises stress slightly greater than the allowable yield strength of the material, 51.5 ksi. Plastic deformation mainly occurred in the two gussets at the U10W node, as shown in Figures 17, 18, and19. Note that any colors other than gray in these figures indicate that the allowable yield strength has been exceeded. The maximum stress predicted, 65 ksi, occurred on the west face of the east gusset, which corresponded to an equivalent plastic strain (PEEQ) of 2.4%. Therefore, the east gusset was the focus of discussion in the report. Note that the typical mesh size in the highly stressed region was about 0.5 inch, as shown in Figure 3, and no contact was yet defined.

Figure 20 shows the enlarged deformed shape of the two gussets at the end of the analysis. Here the deformation scale factor was 30. The deformed shape indicated that the west face of the diagonal truss U10_L9W moved transversely outward of the bridge while the east face of the truss U10_L9W moved transversely towards the bridge.

Figure 21 gives the evolution of the von Mises stress on the west face of the east gusset through the three loading steps. The largest stress always occurred on the edge of the top right fastener connecting the east gusset and diagonal truss U10_L9W. It was clear that the gusset material outside of the top row of fasteners connecting truss U10_L9W yielded even under the original design weight of the bridge, i.e., at the end of step 1. However, only a few elements yielded through the entire thickness. With the application of additional concrete weight and construction loads, more elements yielded through the entire gusset thickness, as shown in Figure 22.

To investigate the stress magnitude's dependency on mesh density, a refined mesh model was also analyzed. The original local model used a typical mesh size of 0.5 inch, as described above and as shown in Figures 3 and 23. The entire model included 694,718 nodes. The maximum stress was predicted to be 65 ksi and the corresponding equivalent plastic strain was 2.4%. The refined mesh model had a typical mesh size of 0.1 inch in the highly stressed region as shown in Figure 24, where the entire model had 1,219,548 nodes. Figures 25 and 26 display the von Mises stress and equivalent plastic strain distributions at the end of analysis for the mesh size of 0.1 inch. The maximum stress was predicted to be 77 ksi and the corresponding equivalent plastic strain was 4.3%. As expected, the finer mesh predicted higher stress. Additional mesh convergence studies could be investigated further using submodeling techniques.

To investigate the effect of contact on stress distribution in the gussets, two models were created. One model had contact defined as shown in Figure 9 while the other model had no contact defined. Other aspects of the two models were the same. C3D8R elements were used to represent gussets. Figure 27 displays the von Mises stress distribution at the end of the analysis in the east gusset for the model with contact defined. The largest stress was predicted to be 60 ksi and equivalent plastic strain to be 1.4%. Figure 28 displays the von Mises stress distribution at the end of analysis in the east gusset for the model without contact defined. The largest stress was predicted to be 65 ksi and equivalent plastic strain to be 2.3%. Thus, the addition of contact

resulted in slightly smaller stress magnitudes. More complex contact involving actual rivets and holes could be investigated further using submodeling method.

Table 11
Summary of Maximum Gusset Stresses and Equivalent Plastic Strain

Mesh Seed, Element	0.5 inch, C3D20R	0.1 inch, C3D20R	0.5 inch, C3D8R	0.5 inch, C3D8R
Contact Condition	No Contact	No Contact	No Contact	Contact
Max. Gusset Stress	65 ksi	77 ksi	65 ksi	60 ksi
Max. Gusset PEEQ	2.4%	4.3%	2.3%	1.4%

Conclusion

Nonlinear finite element analyses have been performed to predict the stress distribution in the gussets at the U10W node of the Minneapolis I-35W bridge under the loadings of original bridge weight, additional concrete weight, and construction loads. The U10W joint was represented by a 3D local model which was embedded into the second (November 2007) global bridge model provided by FHWA.

The analyses predicted initial plastic deformation in the gussets when subjected to the weight of the original bridge design. Plastic deformation in the gussets became more severe with the application of additional concrete weight and construction loads at the collapse. The maximum von Mises stress, 77 ksi at the end of analysis, occurred on the west face of the east gusset and under the edge of the top right rivet connecting the diagonal truss U10_L9W, which corresponded to an equivalent plastic strain of value 4.3%.

References

[1] J. Ocel, “TFHRC Model.pdf”, FHWA, November, 2007.

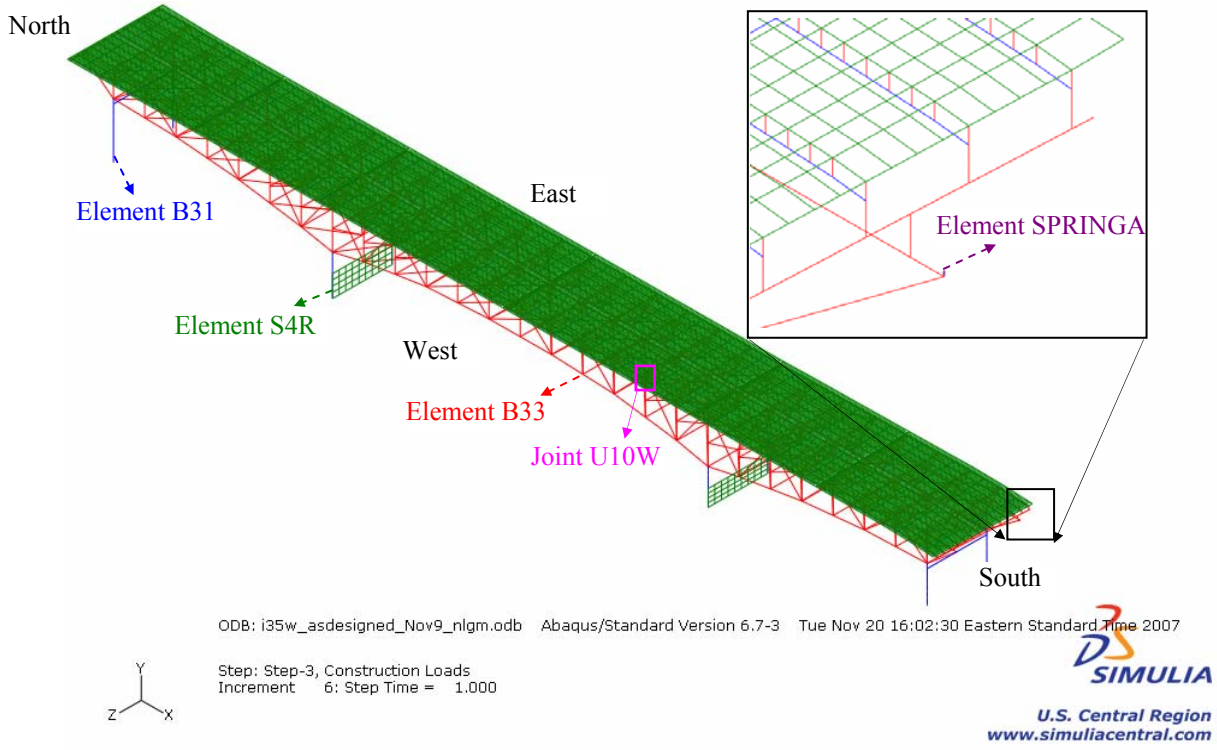

Figure 1: Second bridge model provided by FHWA, November 2007

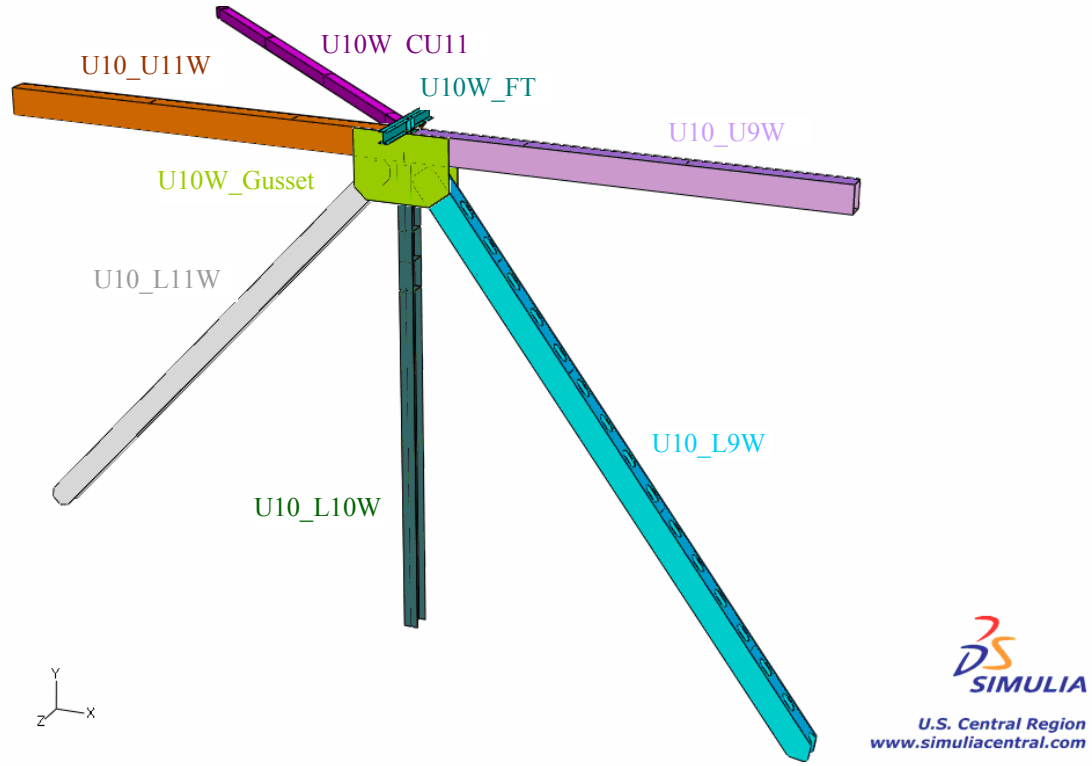

Figure 2: CAD model of the gusset joint at the U10W node

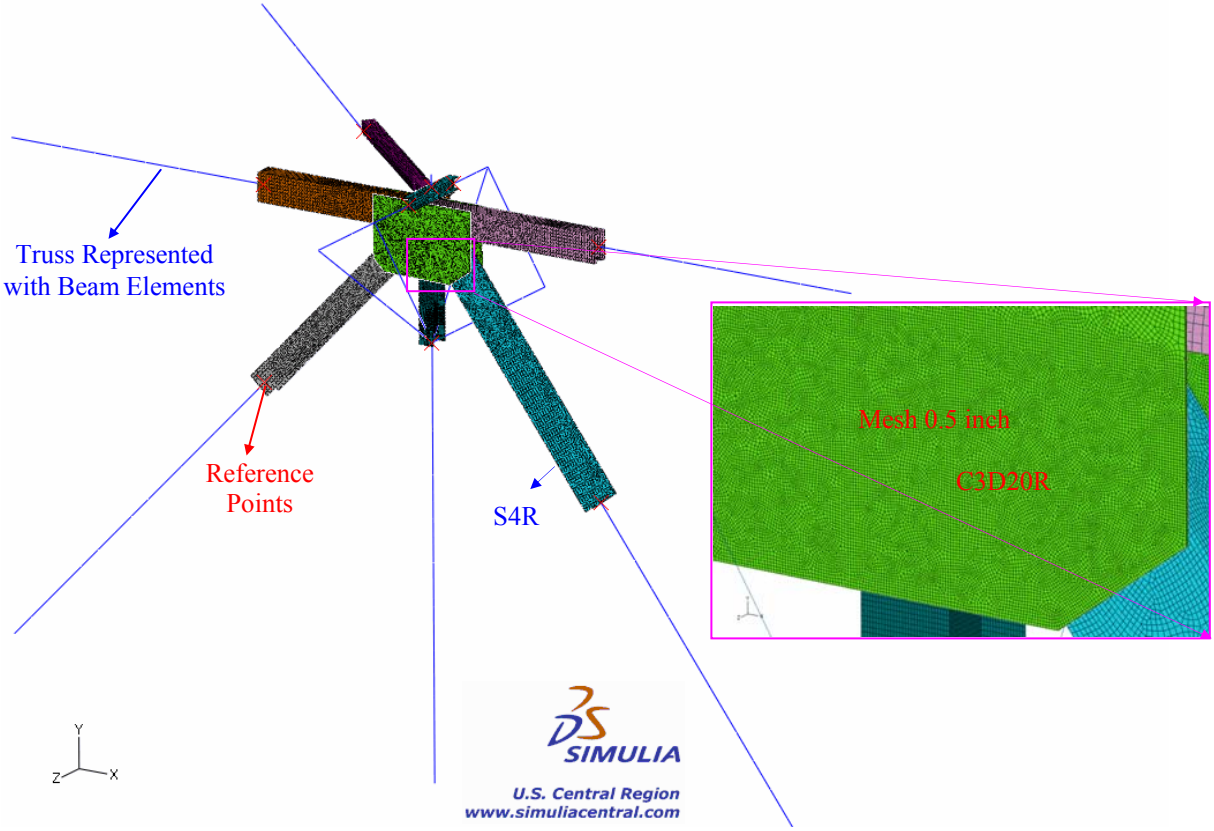

Figure 3: CAE model of the gusset joint at the U10W node

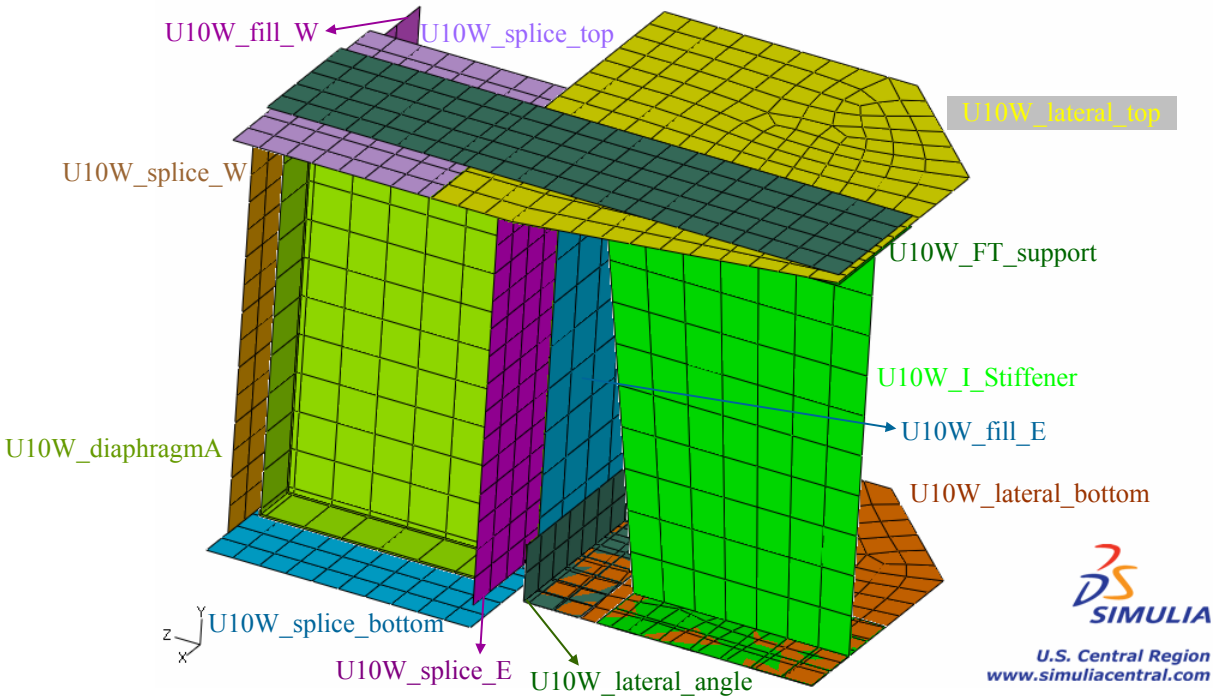

Figure 4: CAE model of connecting plates

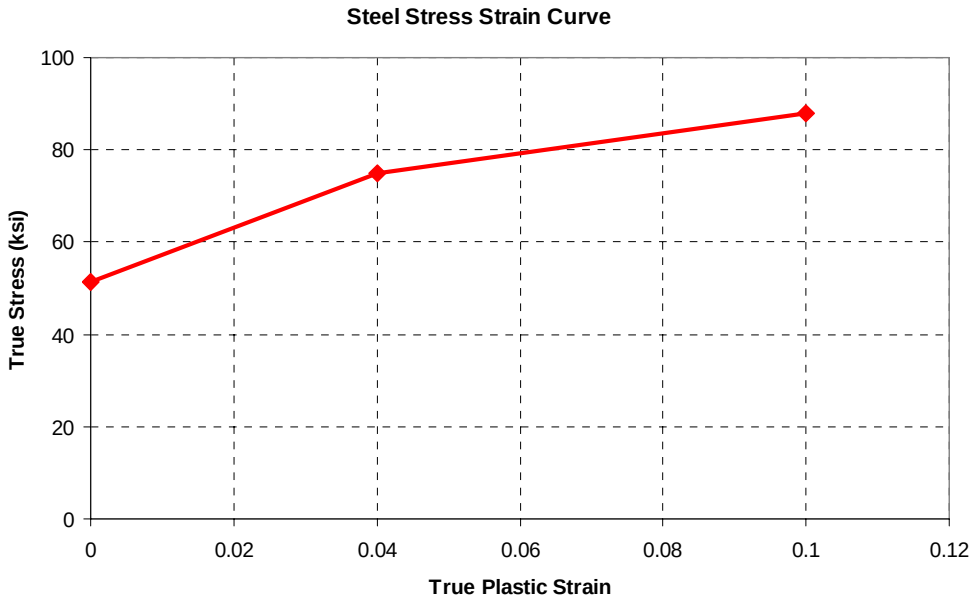

Figure 5: The stress-plastic strain curve of steel

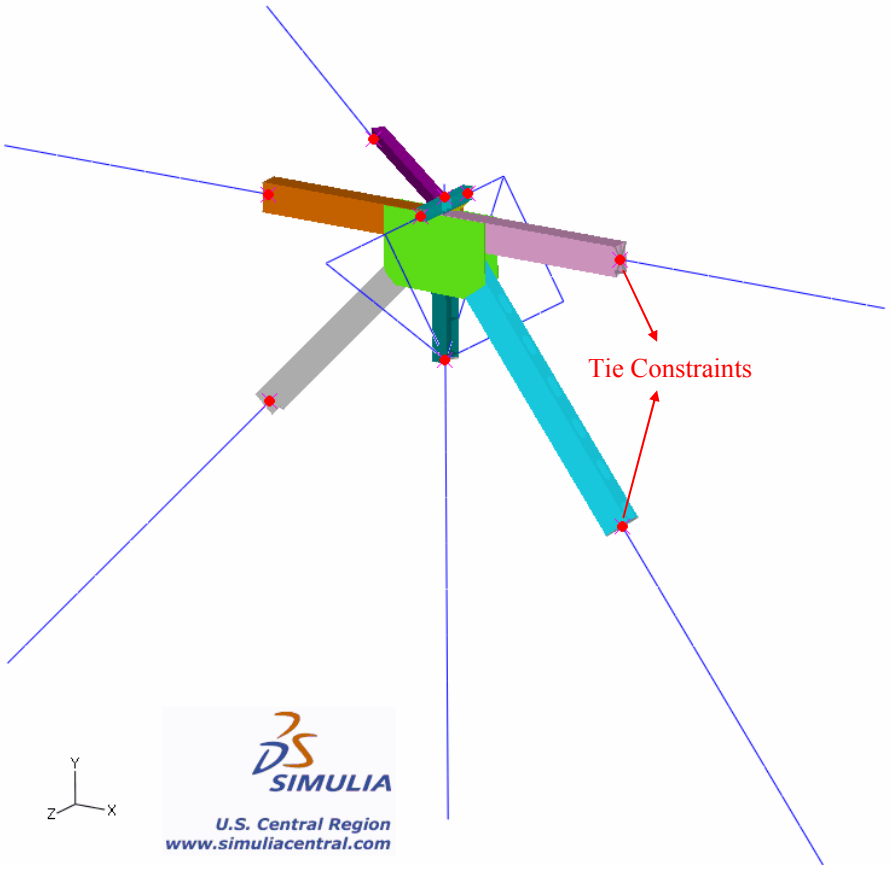

Figure 6: Tie constraints between reference points and global nodes

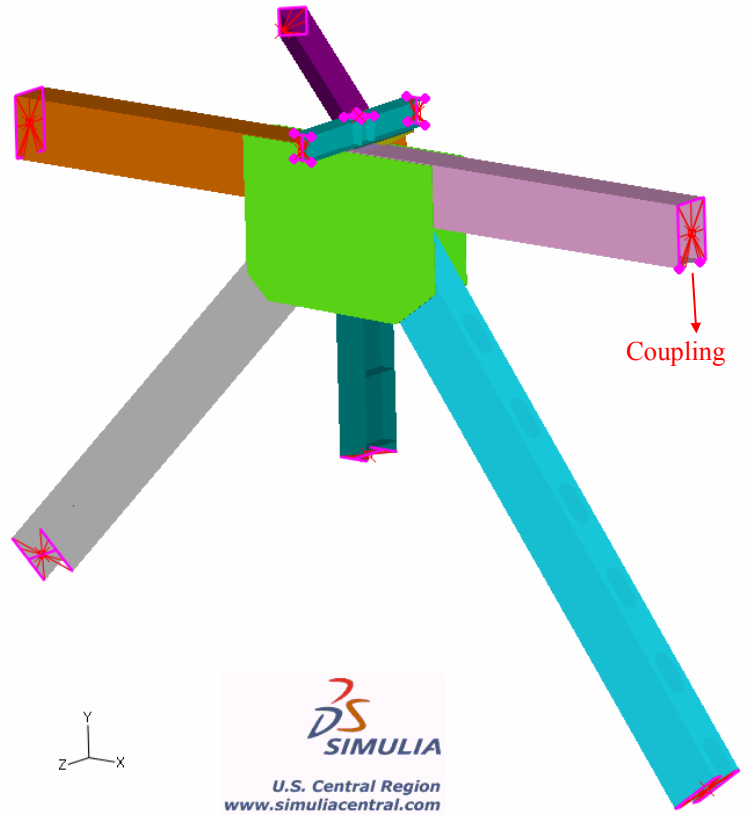

Figure 7: Coupling between reference points and shell cut planes

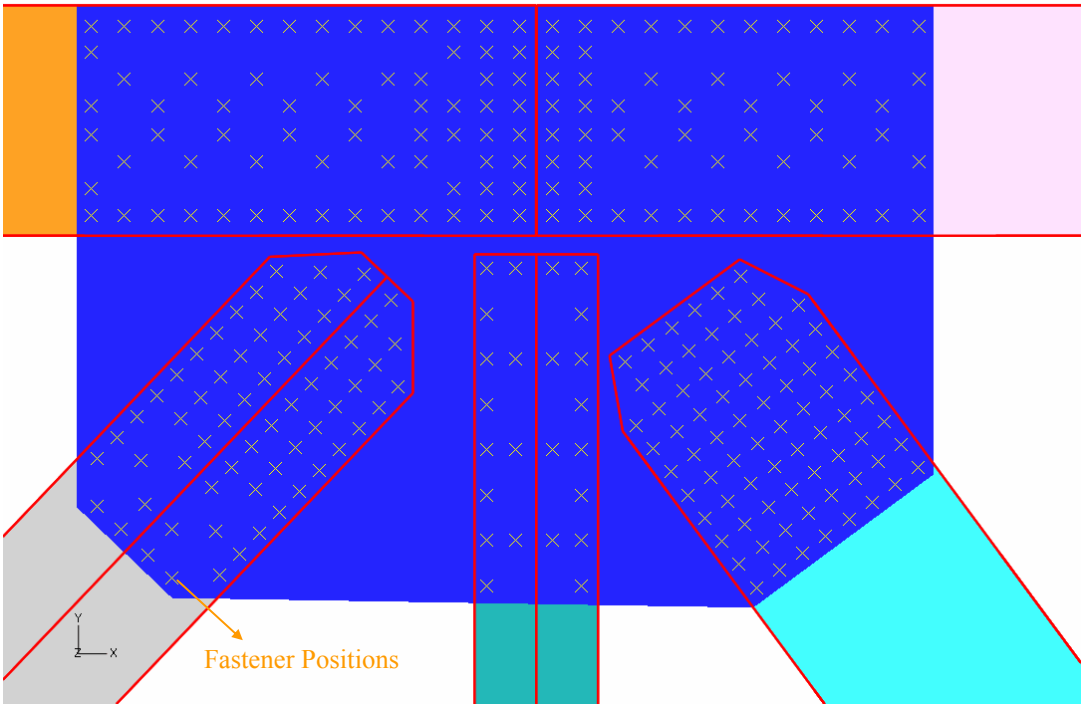

Figure 8: Fastener positions on gusset plate and five main trusses

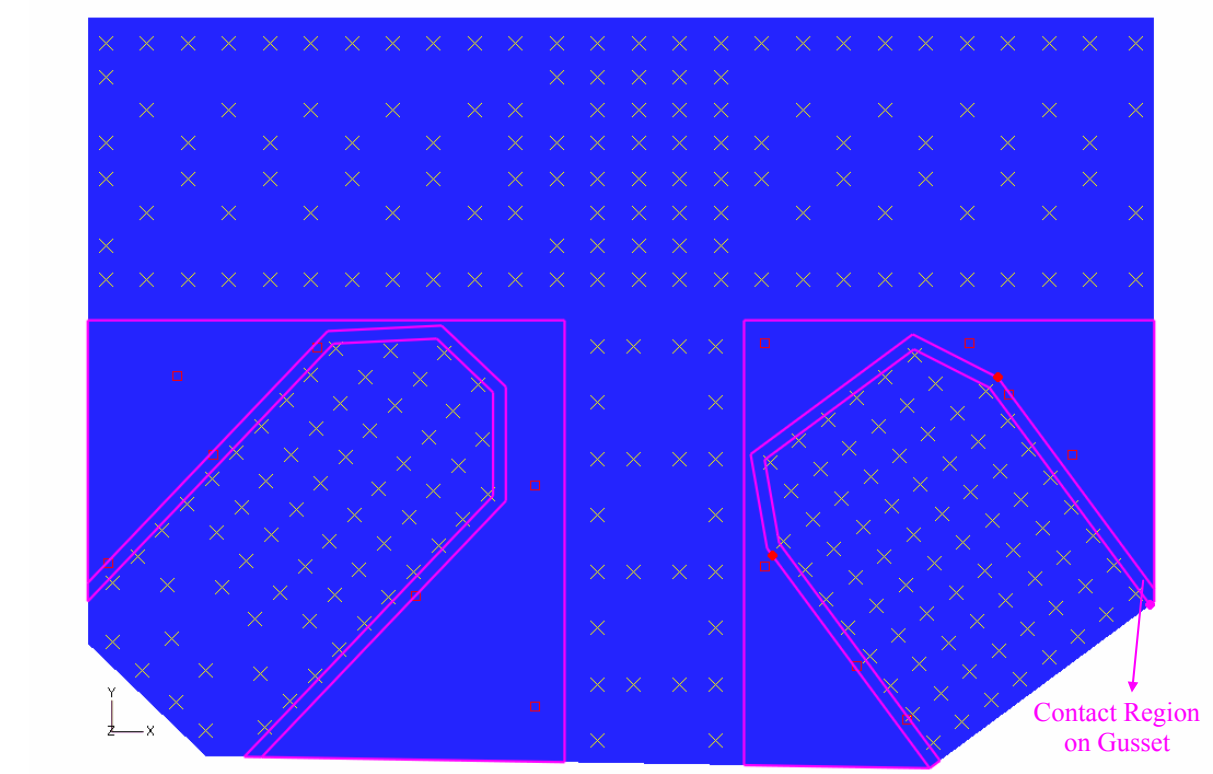

Figure 9: Contact regions defined between gussets and diagonal truss perimeters

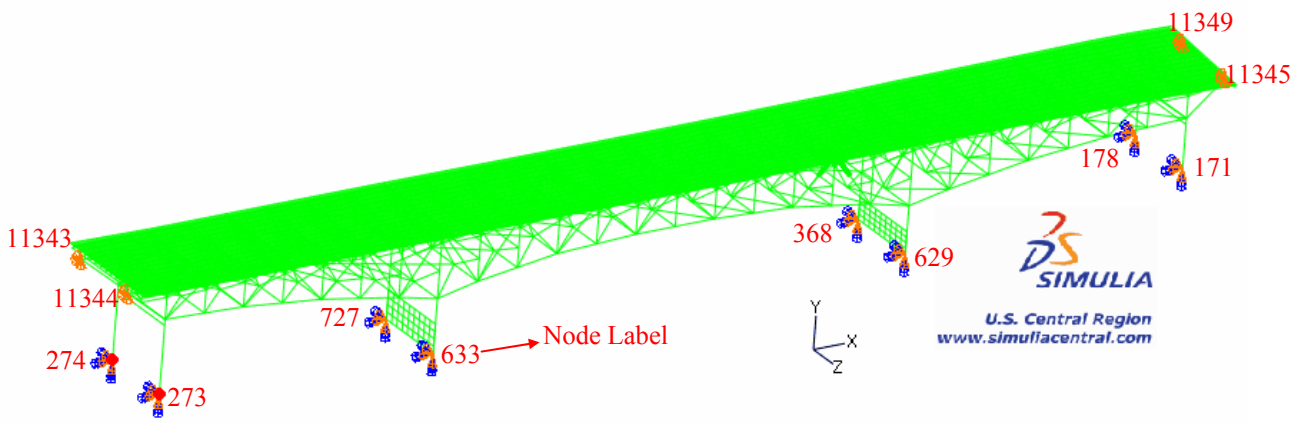

Figure 10: Boundary conditions in step 3

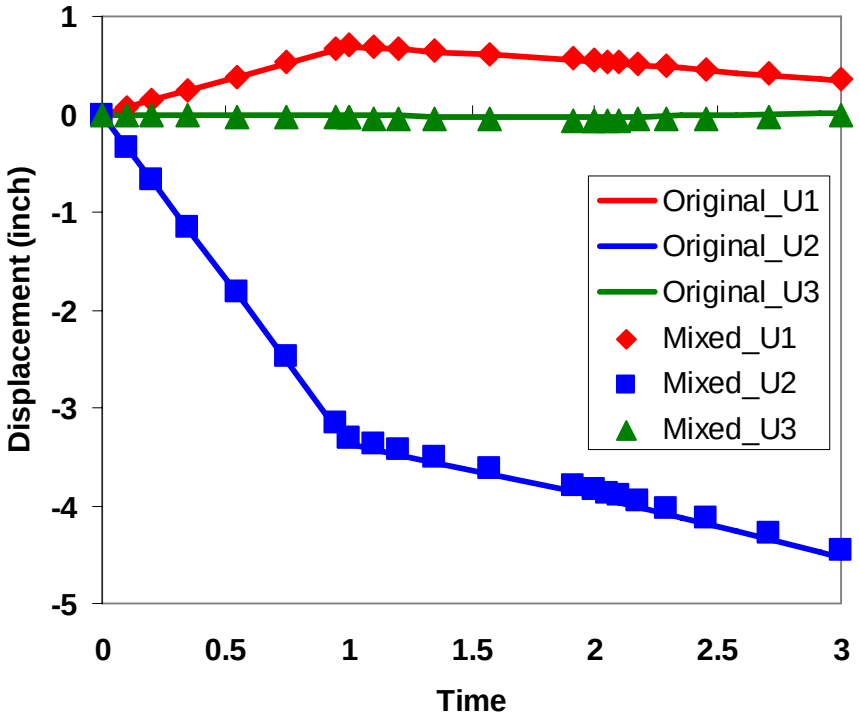

Figure 11: Node U10W translational displacement comparison between original & mixed models

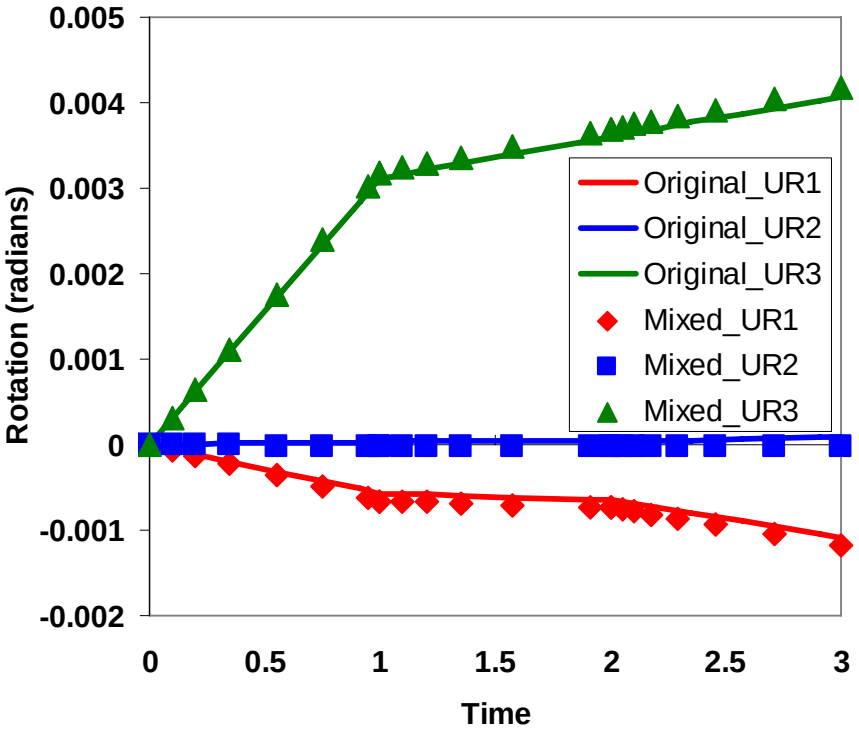

Figure 12: Node U10W rotational displacement comparison between original & mixed models

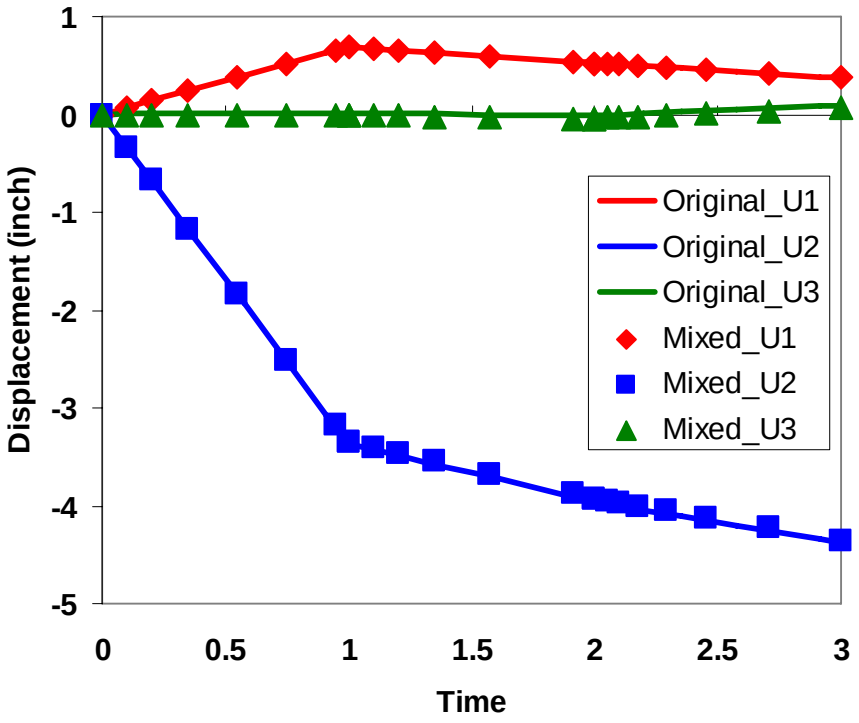

Figure 13: Node U10E translational displacement comparison between original & mixed models

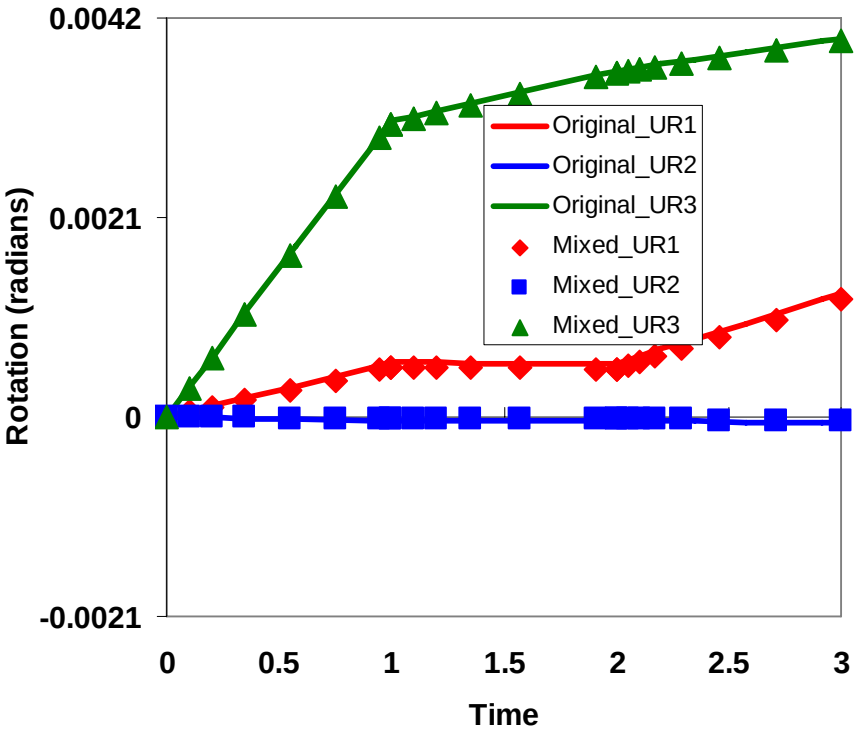

Figure 14: Node U10E rotational displacement comparison between original & mixed models

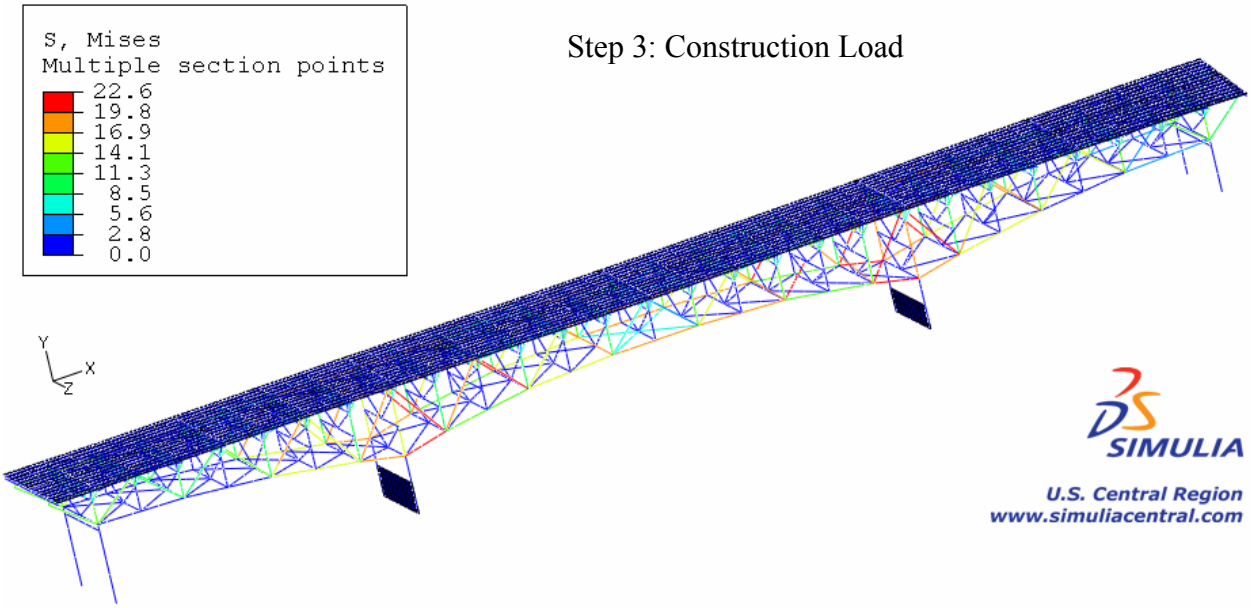

Figure 15: von Mises stress distribution in the global bridge model

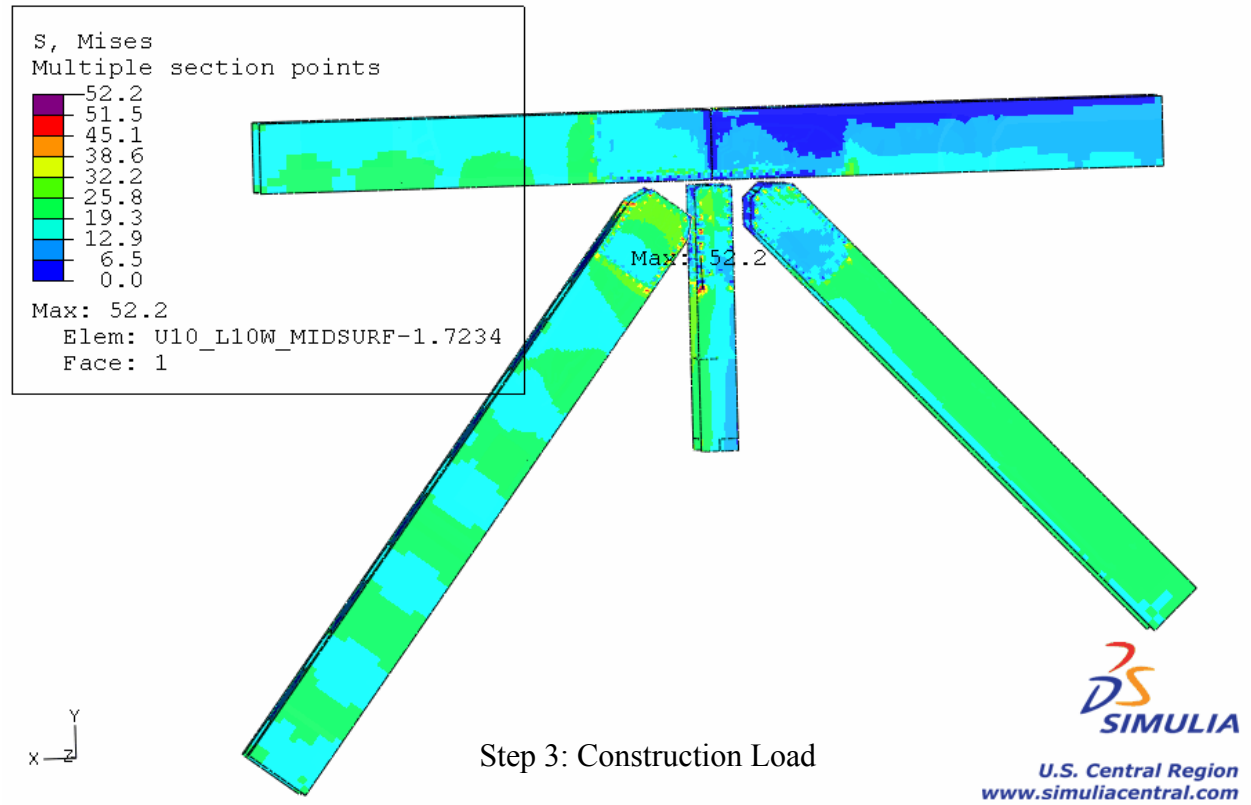

Figure 16: von Mises stress distribution in the five main trusses at the U10W node

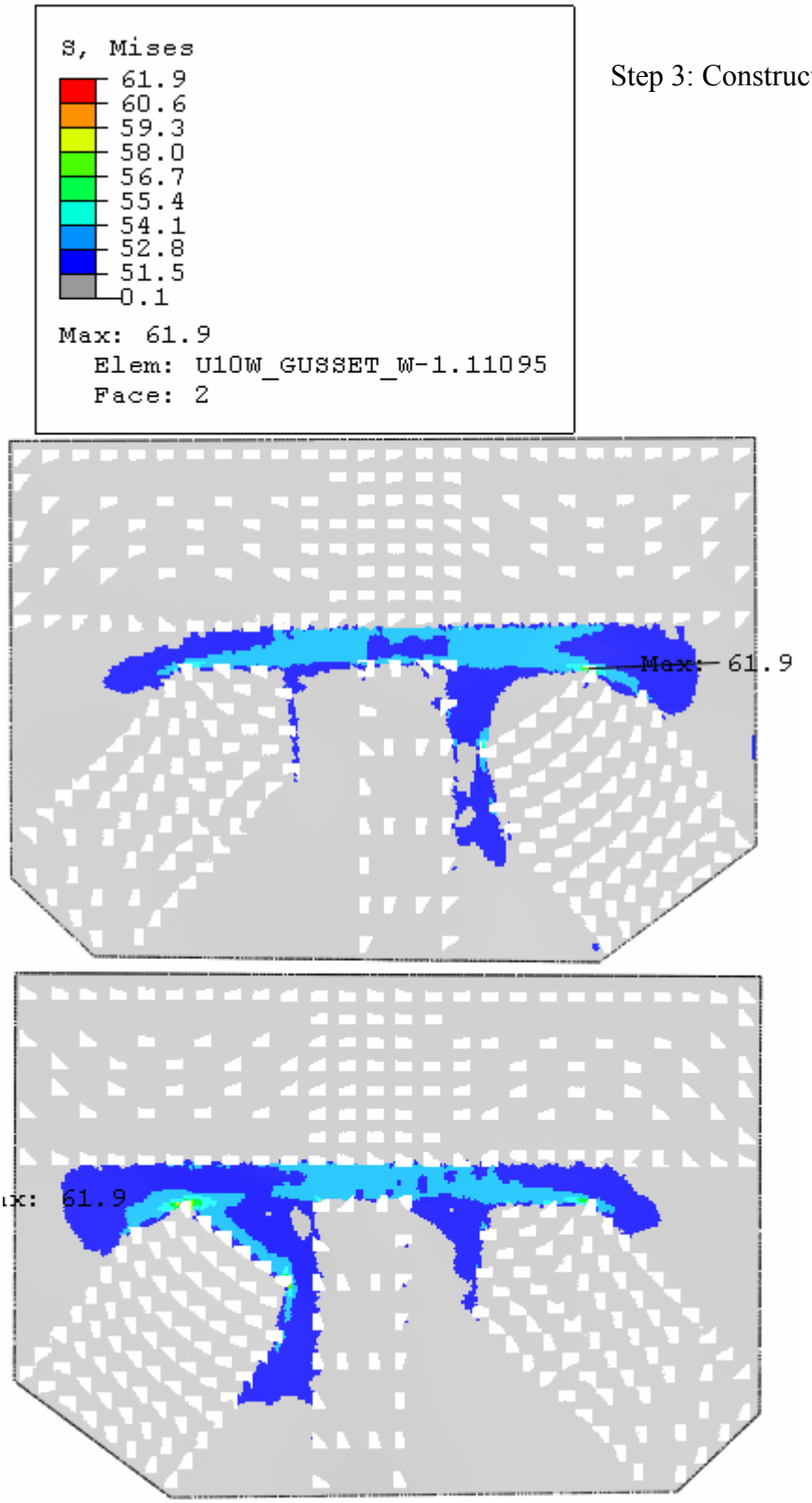

Figure 17: von Mises stress distribution in the west gusset at the U10W node

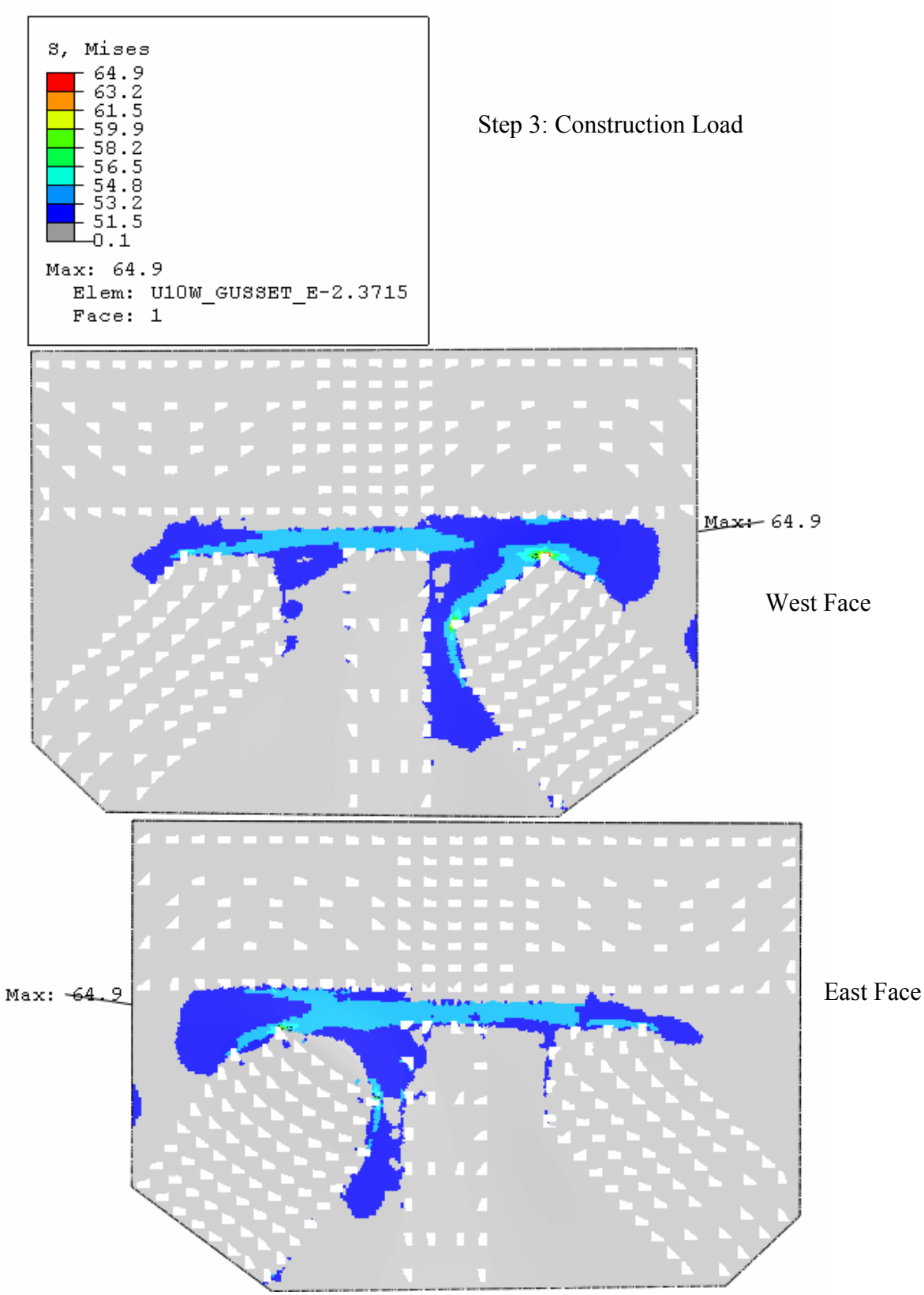

Figure 18: von Mises stress distribution in the east gusset at the U10W node

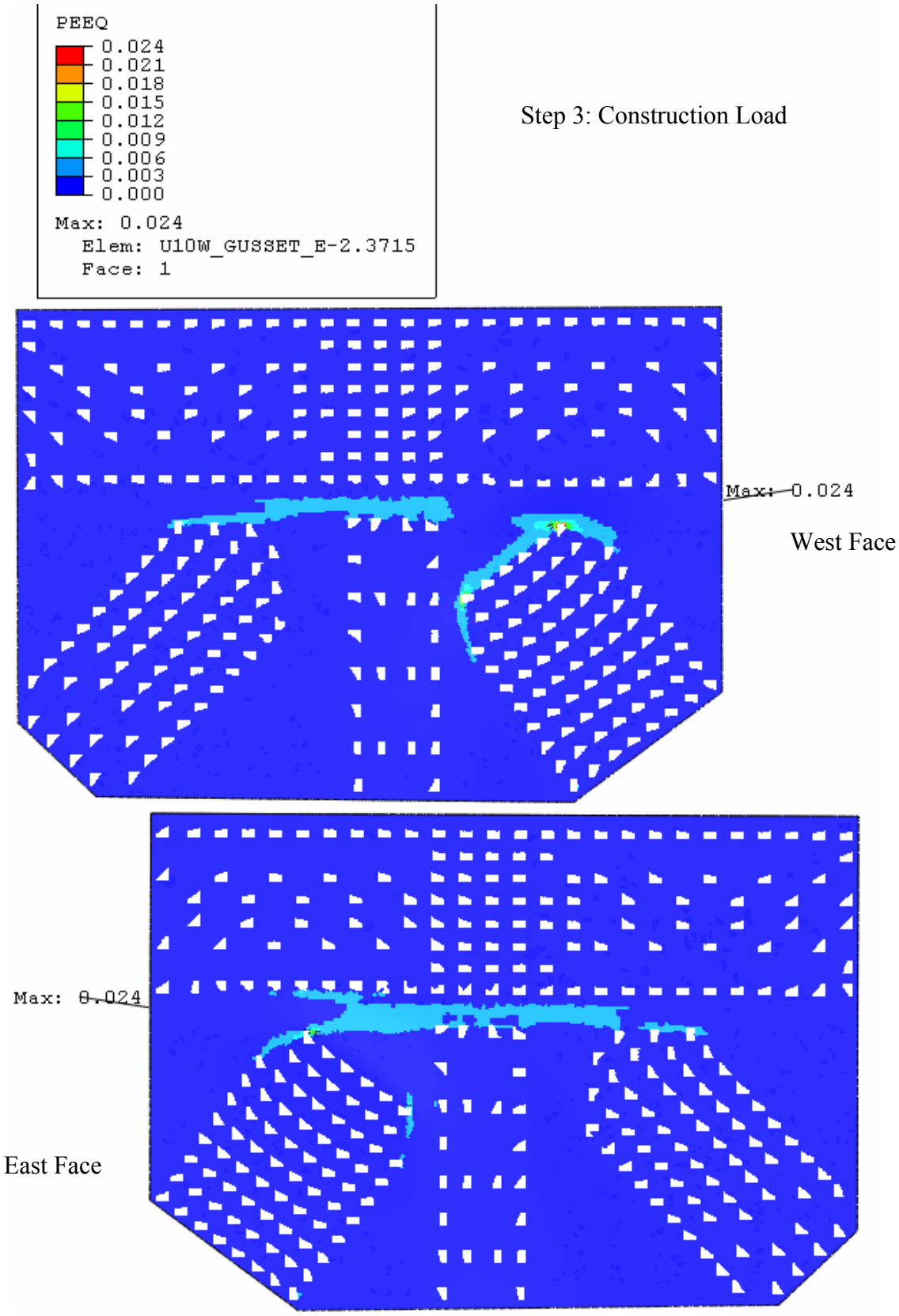

Figure 19: Equivalent plastic strain (PEEQ) distribution in the east gusset at the U10W node

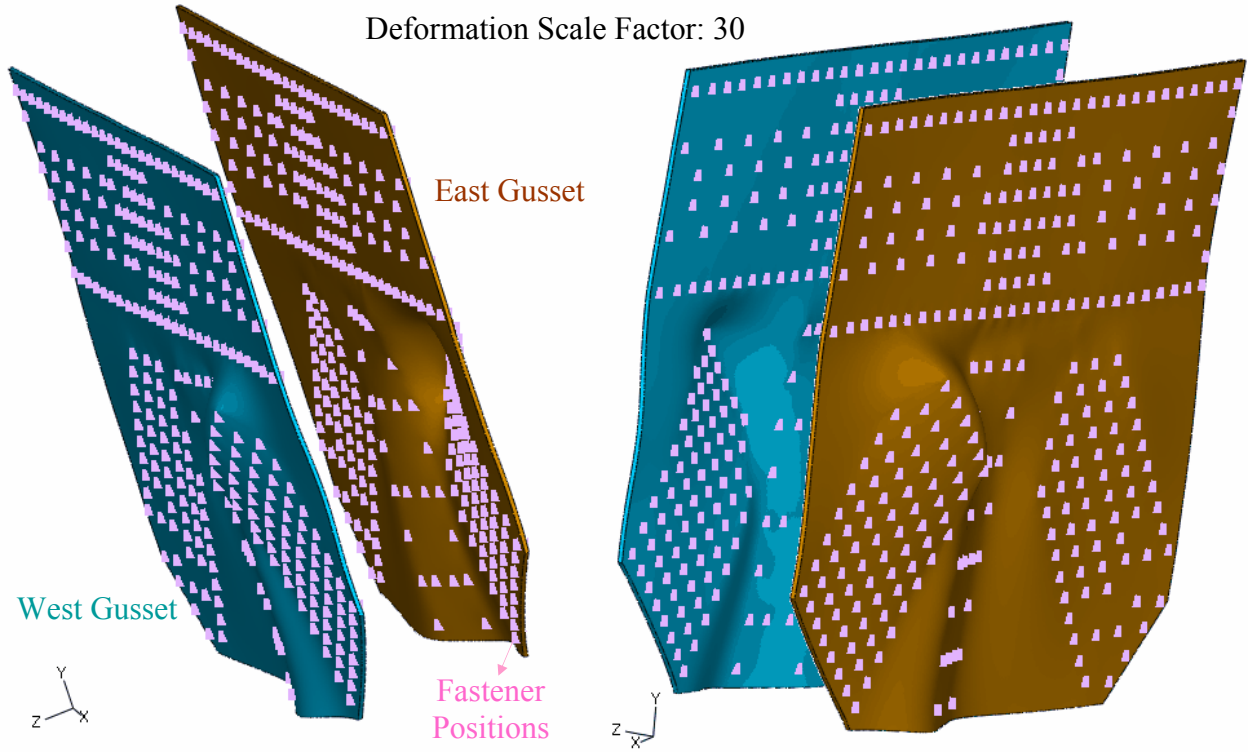

Figure 20: Deformed shape of the gussets at the end of analysis (magnified 30x)

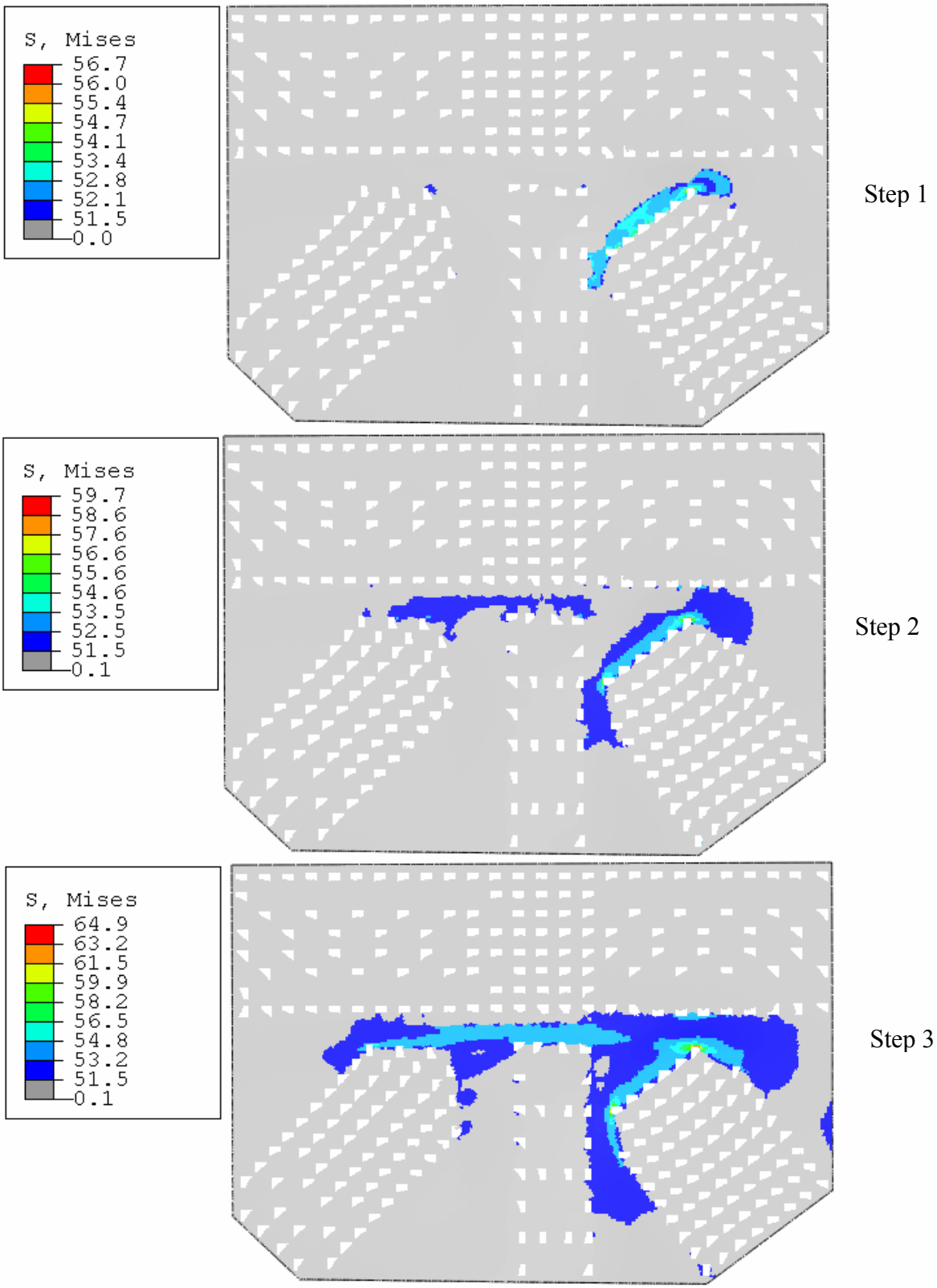

Figure 21: von Mises stress evolution on the west face of the east gusset at the U10W node

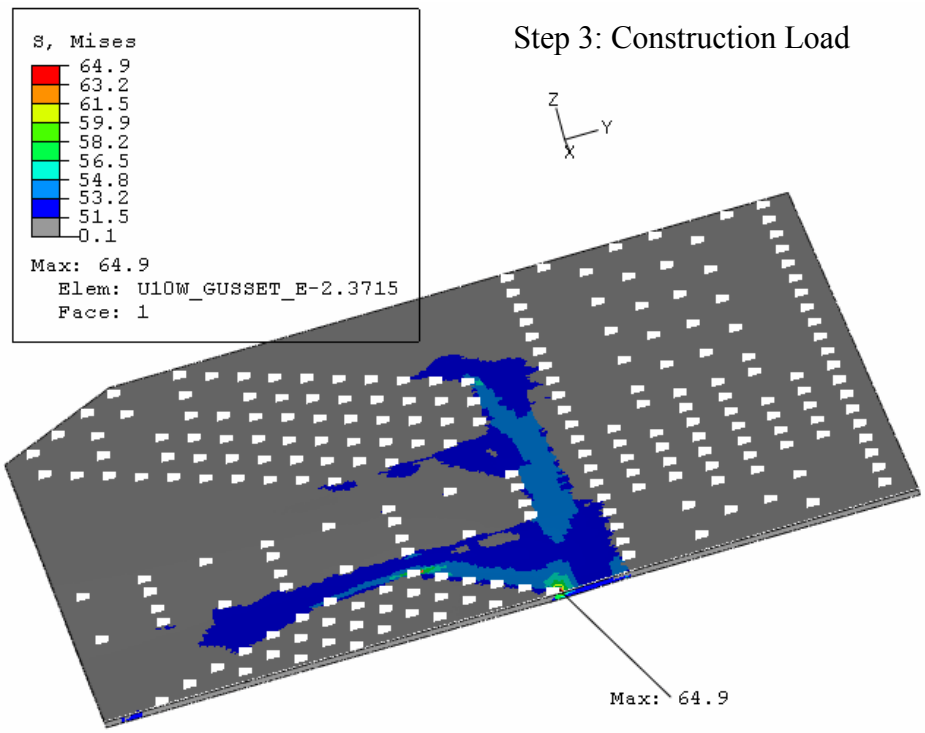

Figure 22: von Mises stress distribution through thickness in the east gusset at the U10W node

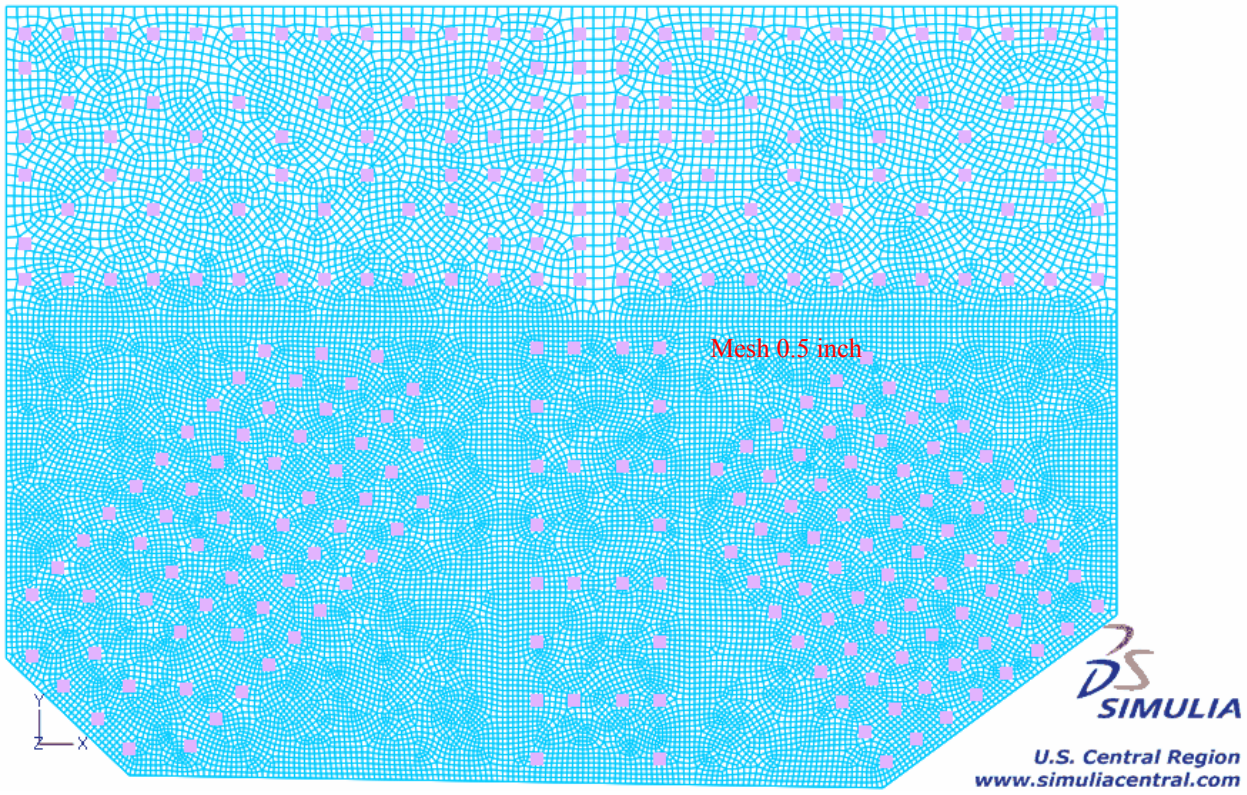

Figure 23: Gusset mesh with typical size of 0.5 inch in highly stressed region

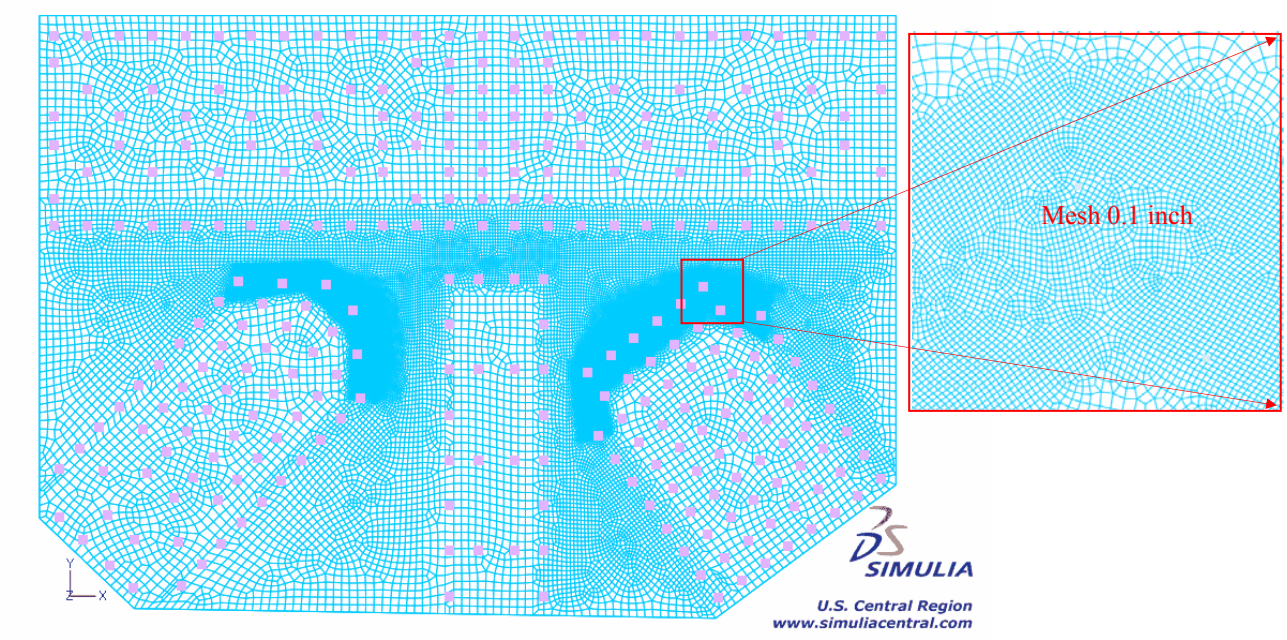

Figure 24: Gusset mesh with typical size of 0.1 inch in highly stressed region

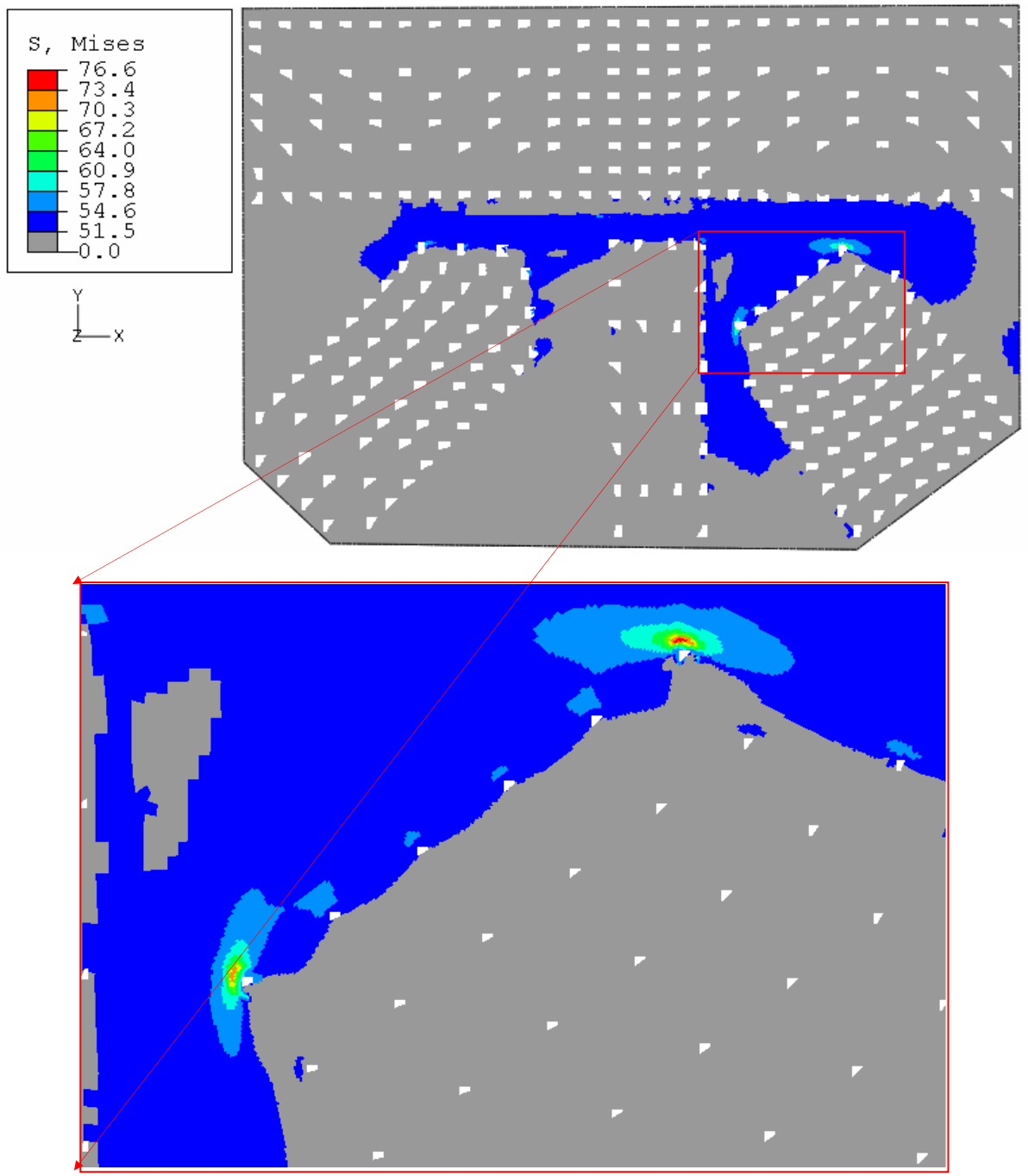

Step 3: Construction Load

Figure 25: von Mises stress in the east gusset with mesh size of 0.1 inch at the U10W node

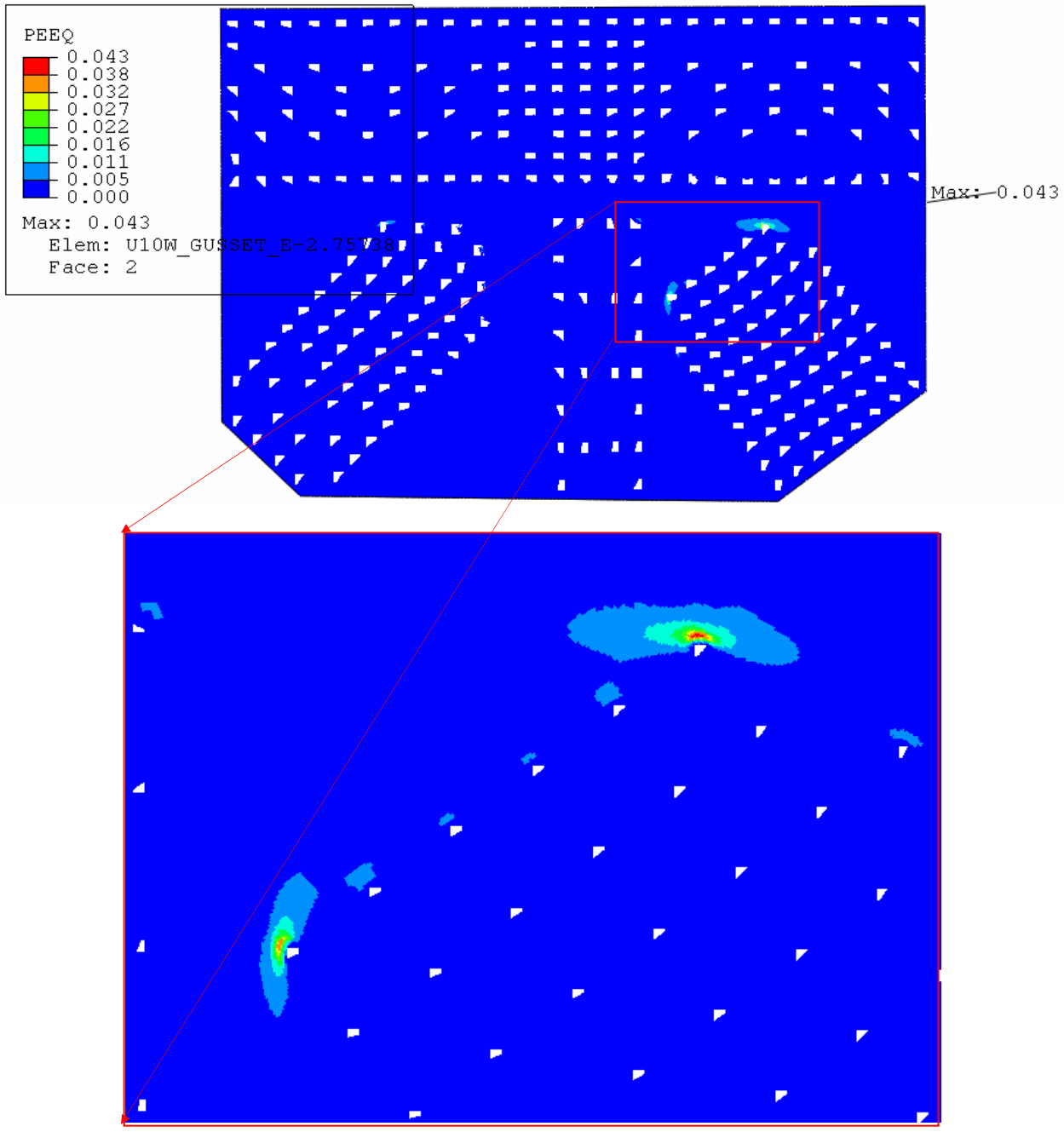

Step 3: Construction Load

Figure 26: PEEQ in the east gusset with mesh size of 0.1 inch at the U10W node

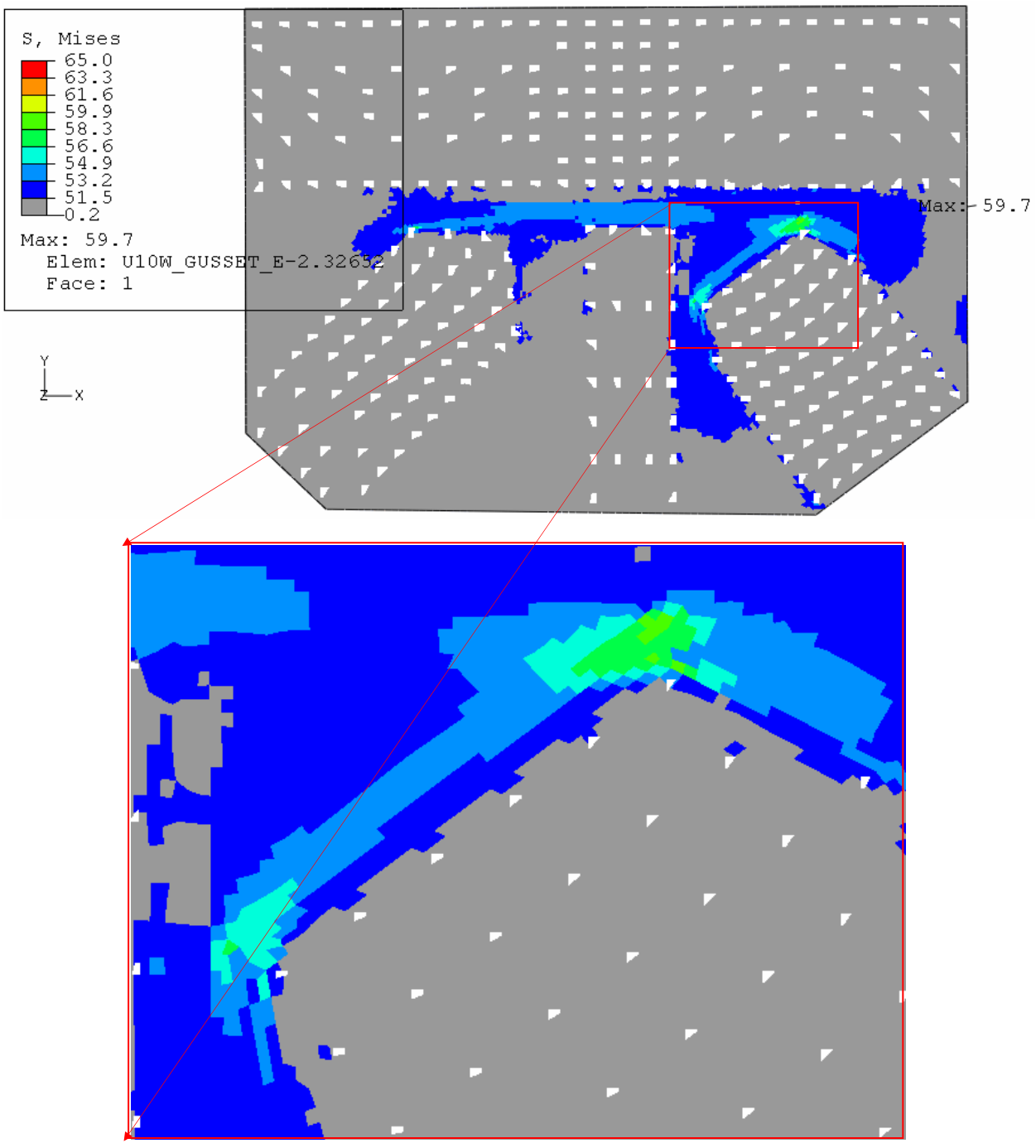

Step 3: Construction Load, Typical Mesh Size 0.5 inch, C3D8R Element for Gussets

Figure 27: von Mises stress in the east gusset at the U10W node with contact defined

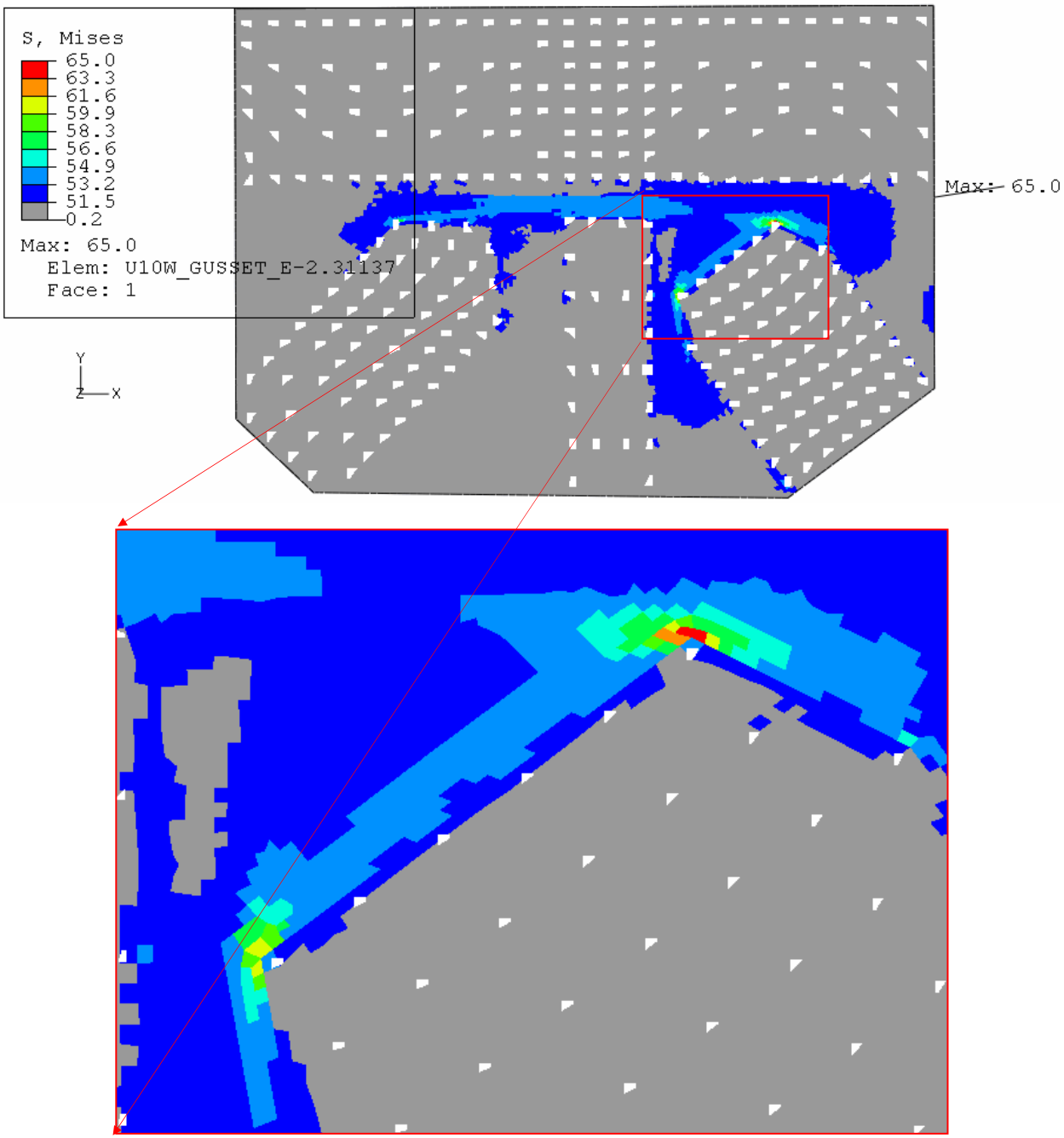

Step 3: Construction Load, Typical Mesh Size 0.5 inch, C3D8R Element for Gussets

Figure 28: von Mises stress in the east gusset at the U10W node without contact defined